4. Using AI for tool wear monitoring during hard turning

4.1 Preface

This chapter describes the development of a tool wear monitoring method for hard turning. Hard turning is used in the manufacturing industry as an economic alternative to grinding. Unfortunately, the reliability of hard turning processes are often unpredictable. One of the main factors affecting the reliability of hard turning is tool wear. Conventional wear monitoring systems for turning operations cannot be used for monitoring hard turning tools because a conglomeration of phenomena like chip formation, tool wear and surface finish during hard turning exhibit unique behaviour compared to regular turning operations. During this research, various aspects connected to hard turning were studied with the aim to design an accurate and reliable tool wear monitoring system for hard turning. From this experience it was clear that the best method to monitor tool wear during hard turning is by means of an Artificial Intelligence (AI) approach.

4.1.1 Introduction to hard turning

Accurate monitoring of the hard turning process is essential to ensure part quality. Experience from industry and various research papers have shown that reliable tool wear monitoring during hard turning processes is even more difficult to achieve than wear monitoring during regular turning operations. Influences of changing machining parameters and disturbances on the process are unpredictable. It is the aim of this chapter to present a new methodology for monitoring tool wear during hard turning. To attain a deeper understanding of the hard turning process, some general observations are necessary: It is known that the tool flank wear in hard turning has a major influence on the surface- and subsurface quality of the workpiece, but crater wear governs the reliability of the operation. Crater wear eventually leads to fracture of the tool. Diffusion and chemical reactions are responsible for the crater wear in hard turning. Major wear on the tool flank can also cause formation of the so-called white layer. White layers are the result of microstructural alteration in the workpiece subsurface. It is called the 'white' layer because it appears white under an optical microscope, and has higher hardness than the bulk material [140,213]. Another phenomenon common to hard turning is material side flow, and is caused by tool wear. Material side flow is the flow of workpiece material opposite to the feed direction due to the high temperatures caused by the process. This affects the quality of the finished workpiece. Material side flow is also influenced by cutting speed, and will increase with increasing tool wear [214].

4.1.2 Tool wear with relevance to hard turning

Dawson and Kurfess [215] investigated the wear trends of CBN cutting tools in hard turning. Experiments with different grades of CBN tools were conducted under different cutting conditions. It was found that the specific geometry of the wear on the tool is very important, especially to improve current FEM models of hard turning. It was found that crater wear changes the nominal cutting geometry. It was also found that the flank wear on the same grade of CBN tools under the same conditions differ.

It is unfortunate that experiments were not repeated with the same tools. It was concluded that cutting speed had the most dramatic effect on the tool life, which improved with slower cutting speeds. Significant changes in the cutting geometry were recorded due to flank and crater wear. Zimmermann *et al.* [216] investigated the wear of CBN tools during hard turning using Spectroscopy and X-Ray techniques. In this case, it was concluded that the wear mechanism of the initial crater wear is due to a tribochemical mechanism. The remaining region is then abraded. The wear mechanism for flank wear could not be positively identified.

Chou and Evans [140] also made investigations towards the tool wear mechanisms during hard turning, and found that the carbide sizes of workpieces have a significant effect on fine scale attrition, which appears to have a dominant effect on low CBN content tools. The work was extended to interrupted hard turning and it was shown that tool life is sensitive to cutting speed and rate of interruption [217]. Experiments also revealed that depth of cut has the least influence on surface roughness in hard turning. Generally, it has been found that the thrust force is a good indicator of tool wear in hard turning.

Ozel and Nadgir [218] propose the use of backpropagation NNs for prediction of the flank wear during hard turning. Orthogonal cutting tests were performed using a dynamometer that can collect the torque and the three component cutting force. A force ratio and cutting conditions are included in the input layer; the hidden layer has 30 neurons and the output layer consist of 8 neurons, which is a binary representation of the experimentally measured flank wear. Interestingly, the use of a predictive model is also described to calculate the force ratios for cutting conditions that were not included in the experiment. Good results for flank wear predictions were obtained using the NN approach. The authors want to extend the work to a sensorless approach for on-line TCM, which in the opinion of this author will yield only a tool life equation based on NNs, and will be of limited use.

The scope of this chapter is to develop a monitoring system for hard turning by using a dynamic AI technique, such as dynamic NNs. Passive modelling of manufacturing operations does not meet the requirements for an industrial system. Kothamasu and Huang [219] identified the same problem and developed a dynamic method for hard turning using Neuro-Fuzzy modelling. In this chapter, another method is proposed based on a combination of static and dynamic NNs.

4.2 Experimental setups

4.2.1 Physical configurations

A total of eight experiments were conducted, all with the same basic configuration. However, in order to isolate disturbances and to identify appropriate features for monitoring, some of the experimental conditions were varied. Thus, care was taken to ensure that all experimental conditions remain the same, except parameters that were controlled changes. The basic configuration is shown diagrammatically in Figure 4.1. It consisted of a CNC turning machine equipped with a tool holder dynamometer for 3-component cutting force measurements. In some experiments, Acoustic Emission (AE), 3-component acceleration and temperature measurements were also made.

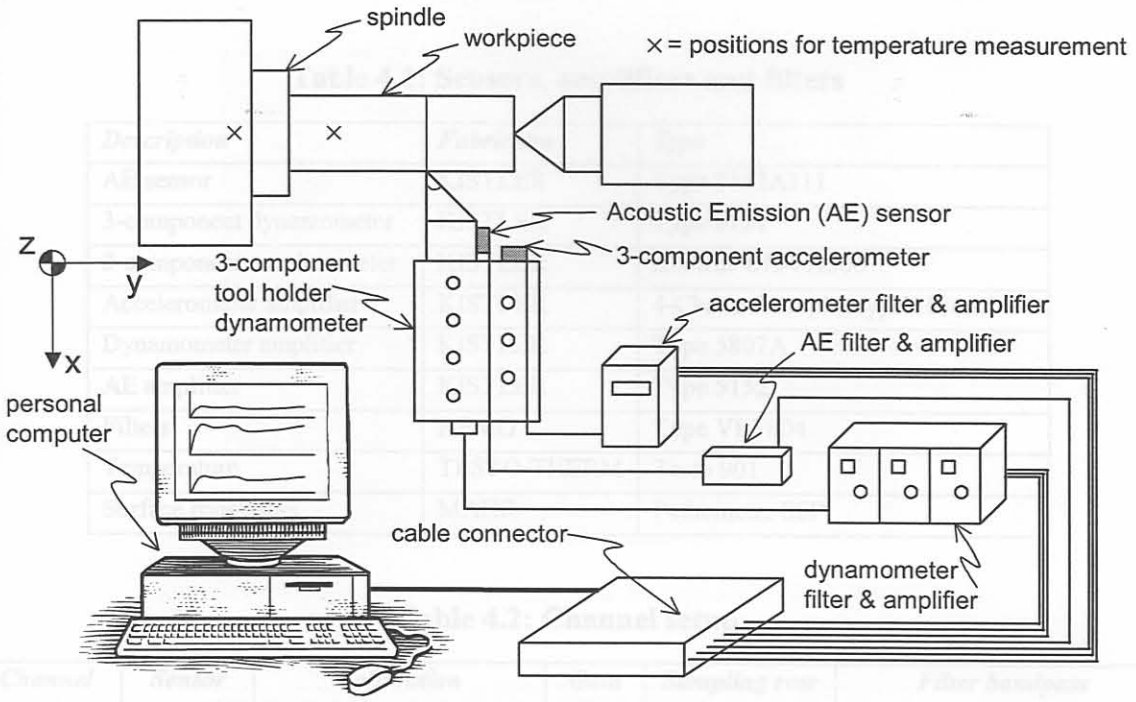

Figure 4.1: Schematic representation of experimental setup

A detailed description of the hardware is given in Table 4.1, with the conditions for each channel in Table 4.2. The variables that were measured during each experiment are summarised in Table 4.3. It is known that the static cutting forces are good indicators of tool wear, but a proper dynamic analysis of the cutting forces can also generate reliable features for wear monitoring. To achieve this, a high sampling rate and analogue low-pass filtering must be used. AE and acceleration also possess properties for wear monitoring during hard turning and these were included during some experiments.

Temperature measurements were made to investigate the effect of fluctuating temperatures on the experimental results. From an industrial point of view, the surface finish of the turned components is the most important feature of the workpiece, and consequently the surface finish of all the workpieces were also measured with a stylus. This enabled an investigation into the effect of tool wear on the surface finish.

In all experiments an analogue trigger was used to start the recordings. In the event where two PCs were used simultaneously the same trigger channel and threshold level were used to ensure alignment of the data. The accelerometer and AE sensor were attached close to the tool tip on the tool holder. The dynamometer was attached on the index turret, and the tool holder containing the CBN insert was clamped in the dynamometer. All sensors are piezo-based, with the dynamometer a special arrangement that can measure both DC and AC signals reliably up to about 1.2 kHz. Many previous studies have found that it is important to mount the AE and vibration sensors as close as possible to the tool tip. In fact, this is more important than the actual mounting orientation, especially in the case of AE.

Table 4.1: Sensors, amplifiers and filters

Description	*Fabricator*	*Type*
AE sensor	KISTLER	Type 8152A111
3-component dynamometer	KISTLER	Type 9121
3-component accelerometer	KISTLER	*K-shear* 8794 A500
Accelerometer amplifier	KISTLER	4-Channel coupler type 5134A1
Dynamometer amplifier	KISTLER	Type 5807A
AE amplifier	KISTLER	Type 5152
Filters	KEMO	Type VBF804
Temperature	TESTO-THERM	Testo 901
Surface roughness	MAHR	Pethometer S8P

Table 4.2: Channel setup

Channel	*Sensor*	*Calibration*	*Gain*	*Sampling rate*	*Filter bandpass*
1	AE_{real}	$57dB_{ref\ 1V/(m/s)}$	10	400 kHz	50 kHz -100 kHz
2	AE_{rms}	$57dB_{ref\ 1V/(m/s)}$	1	20 kHz	50 kHz -100 kHz
3	Fx	50 N/V	1	20 kHz	DC - 3 kHz
4	Fy	50 N/V	1	20 kHz	DC - 3 kHz
5	Fz	50 N/V	1	20 kHz	DC - 3 kHz
6	Ax	10 mV/g	100	20 kHz	10 Hz - 6 kHz
7	Ay	10 mV/g	100	20 kHz	10 Hz - 6 kHz
8	Az	10 mV/g	100	20 kHz	10 Hz - 6 kHz

Table 4.3: Measurements per experiment

	Exp. 1	*Exp. 2*	*Exp. 3*	*Exp. 4*	*Exp. 5*	*Exp. 6*	*Exp. 7*	*Exp. 8*
AE_{real}	✓							
AE_{rms}	✓							
Three cutting forces	✓	✓	✓	✓	✓	✓	✓	✓
Three cutting vibrations		✓	✓	✓				
Surface roughness	✓	✓	✓	✓	✓	✓	✓	✓
Workpiece diameter	✓	✓	✓	✓				
Machine temperature	✓							
Room temperature	✓							
Workpiece temperature	✓							

In the following pages, pictures of the experimental setups are shown. Figure 4.2 is a picture of the machine and the electronic equipment for experiments 1-4. In Figure 4.3 and Figure 4.4 the sensors and workpiece for experiments 1-4 can be seen. The machine used for experiments 4-8 is shown in Figure 4.5. The layout of the workpiece and the dynamometer for experiments 4-8 is depicted in Figure 4.6.

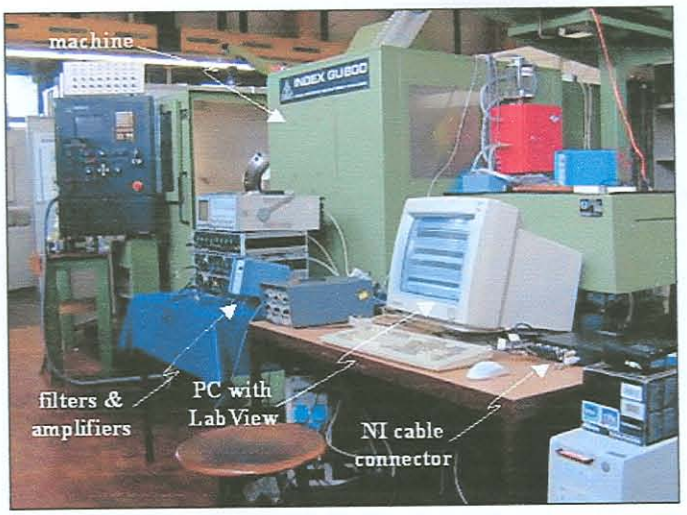

Figure 4.2: Machine and electronic equipment experiment 1-4

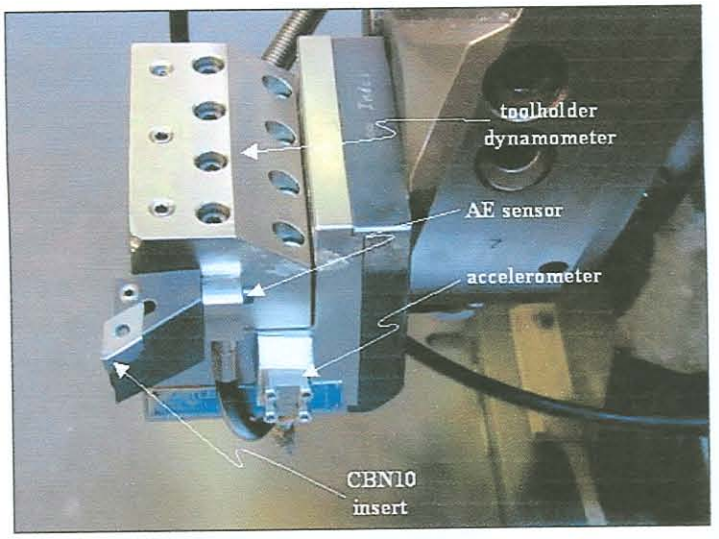

Figure 4.3: Sensors experiment 1-4

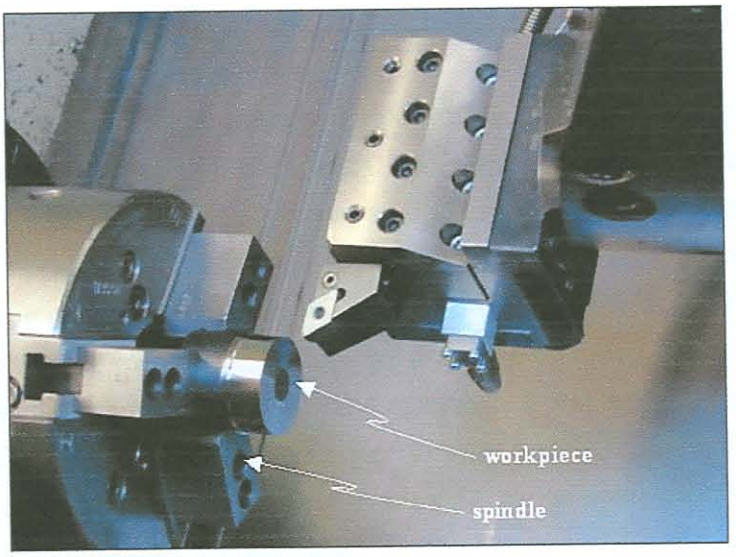

Figure 4.4: Workpiece setup experiment 1-4

Figure 4.5: Machine experiments 4-8

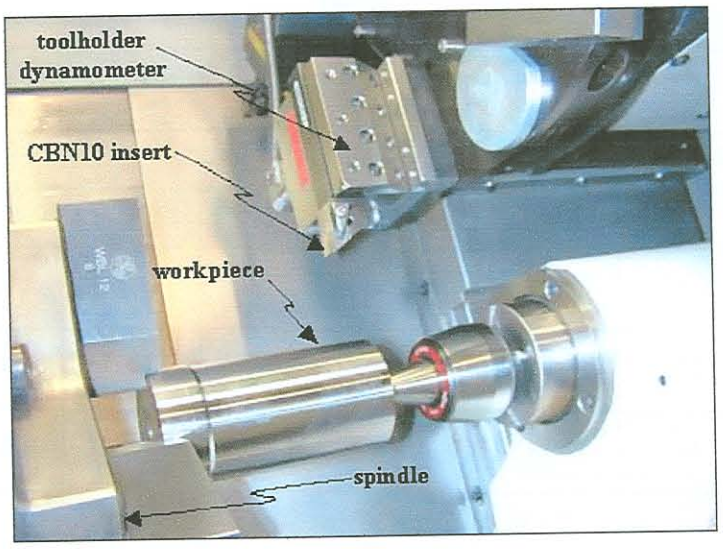

Figure 4.6: Layout of workpiece and dynamometer experiments 4-8

4.2.2 Procedure and process parameters

The experimental procedure consisted of several steps. With each new workpiece, a preparation cut with depth 0.1 mm was made with a preparation tool. This was to ensure that during subsequent runs, a constant depth of cut is maintained. After the preparation cut the workpiece remains in the chuck and the preparation tool is replaced with the tool under test. Also, before each machining test, the temperature of machine, workpiece and room were measured with a temperature probe. Care was taken to measure in the same positions every time. After the runs were completed, the temperature of the machine and workpiece (still clamped) were measured again. Then, the tool was removed for wear measurement under a tool maker's microscope. As a last step the surface roughness of all the workpieces were measured with a stylus. The tempo of the experiments varied somewhat, with some running over several days and others running over a single day.

The machining parameters were selected to resemble industrial practice. The machining parameters for

strategy, experiments were repeated with the same parameters. In essence, the cutting speed and feed rate was varied, and experiments were conducted on two different lathes and workpiece types. Hence, the effect of the machine type, workpiece hardness and geometry can be investigated. The type of tool insert (CBN 10) was not varied, and the depth of cut was kept constant and continuous at 0.1mm for all experiments.

Table 4.4: Experimental parameters

Description	*Exp. 1*	*Exp. 2*	*Exp. 3*	*Exp. 4*	*Exp. 5*	*Exp. 6*	*Exp. 7*	*Exp. 8*
Machine	INDEX GU800				Montforts RNC 400 plus			
Holder	SECO PDJNR/L 2525M11				SECO PDJNER/L 25 25M11			
Insert	SECO DNGA 150612SL1 (CBN 10)							
Depth of cut [mm]	0.1mm							
Speed [m/min]	140						160	
Feed rate [mm/rev]	0.04	0.08				0.16	0.08	0.16
Workpiece	100Cr6				51CrV4			
Passes	210	256	210	216	76			
Total time [min]	74.4	43.0	50.2	50.3	187.0	91.7	157.4	77.1
Total length [km]	10.42	6.01	7.03	7.04	26.18	12.84	25.18	12.34
Diameter [mm]	41.7	40.7	41.8	40.6	72.8	72	71.2	70.4
Pass length [mm]	15		20		120			

4.2.3 Method for tool wear measurement

A combination of flank and crater wear governs the hard turning process. In order to correlate the sensor information with the formation of tool wear, tool wear measurements were made between each new workpiece. The shape of the wear was described with the parameters depicted in Figure 4.7. These are:

VB_{avg} - Average flank wear
VB_{max} - Maximum flank wear
VB_L - Approximate length of the flank wear
K_W - Width of the crater wear
K_D - Depth of the crater wear
K_L - Approximate length of the crater wear

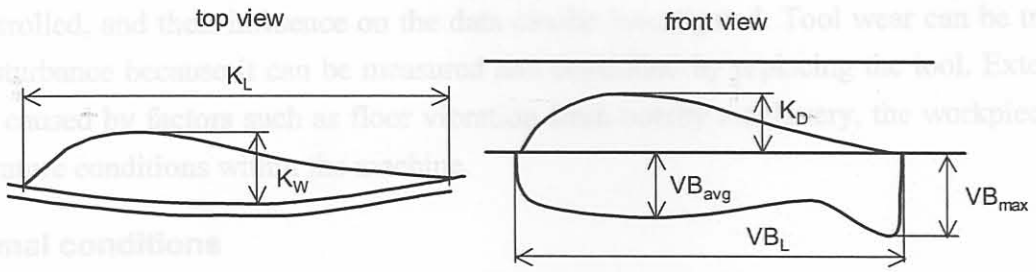

Figure 4.7: Tool wear parameters

For the purpose of the NN implementation, it was decided to attempt to describe to flank wear in terms of an approximate area of flank wear, and the crater wear in terms of an approximate volume of crater wear. Though these are very crude approximations, it is a step in the right direction for more accurate monitoring of tool wear during hard turning. The parameters were formulated as follows:

Area of flank wear:

$$VB_A = VB_{avg} \times VB_L \tag{4.1}$$

Volume of crater wear:

$$K_V = K_W \times K_D \times K_L \tag{4.2}$$

4.2.4 Discussion

The experimental procedures were selected to enable the design of a proper methodology for monitoring tool wear during hard turning that can eventually be treated as a general case. A further reason for the selected experiments was to properly identify and isolate disturbances on the process and experimental setup. The identification of disturbances is a very important issue when monitoring systems for tool wear are concerned. It is known that tool wear will cause a change in sensor signals, but it is extremely difficult to establish whether a change is caused by the tool wear or some other influence on the process (or even something inherent to the experimental setup). Disturbances often have a large influence on the measured signals, whereas the effect of tool wear is relatively small. Several processing methods were used, and are discussed in the following sections.

4.3 Experimental results - disturbances

4.3.1 Introduction

Due to the very small depth of cut, the cutting forces during hard turning are low compared to regular turning. Many studies only consider optimising the hard turning process, such as investigating the lifetime of different tools, analysing the surface and subsurface of hard turned pieces, investigating the influence of interrupted cutting on tool life, *etc.* The purpose of these experiments was to determine which parameters could be used to monitor the tool wear, and identify disturbances on the tool wear data. Methods to treat the effects of disturbances should then be employed.

Disturbances are not only phenomena common to the shop floor but can also be caused by the way in which experiments are conducted in the laboratory. Internal disturbances are caused by known settings inherent to the process, *e.g.* machining parameters. Internal disturbances can be modelled because they

can be controlled, and their influence on the data can be investigated. Tool wear can be treated as an internal disturbance because it can be measured and controlled by replacing the tool. External disturbances are caused by factors such as floor vibration from nearby machinery, the workpiece clamping and temperature conditions within the machine.

4.3.2 Normal conditions

Figure 4.8 shows a typical measurement of cutting forces, with the corresponding Gabor spectrogram (up to 40 Hz) presented in Figure 4.9. It is clear that the forces consist of a static part (DC value) and a dynamic part (AC values). Both the static and dynamic parts of cutting forces are important for TCM [41].

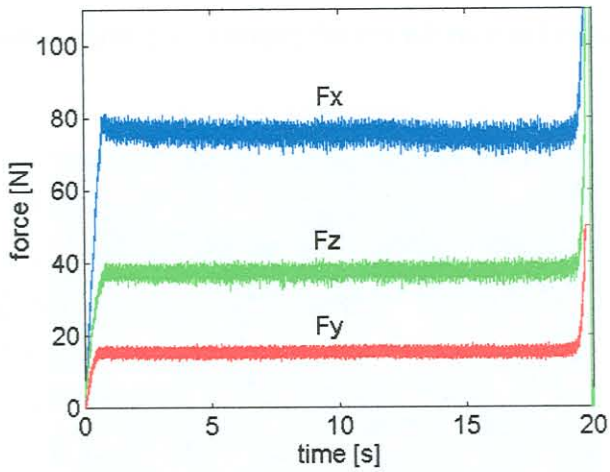

Figure 4.8: Response history of forces under normal conditions

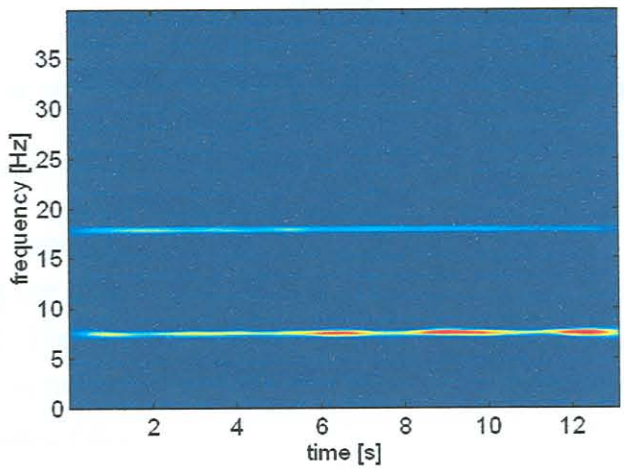

Figure 4.9: Gabor spectrogram of thrust force under normal conditions

4.3.3 External disturbance - clamping condition

In some cases, the workpieces were clamped marginally skew, and this has a big influence on the cutting forces. This influence was taken into account during analysis of the signals. The effect can be monitored by a frequency domain analysis of the cutting force, and was removed from the signal with digital filters. An example of such a measurement is presented in Figure 4.10, with its Gabor spectrogram shown in Figure 4.11.

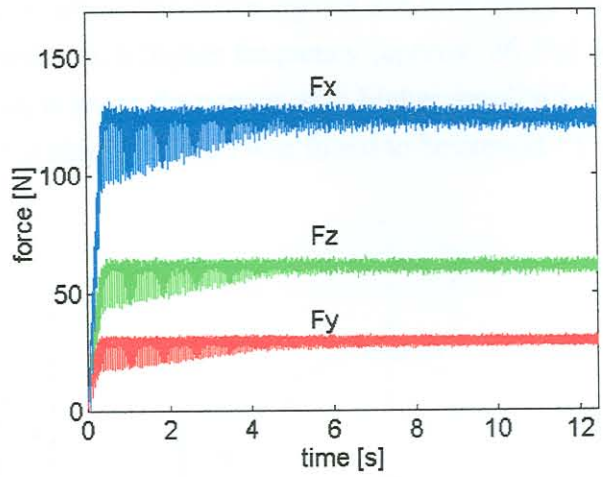

Figure 4.10: Response history of cutting forces when workpiece is clamped skew

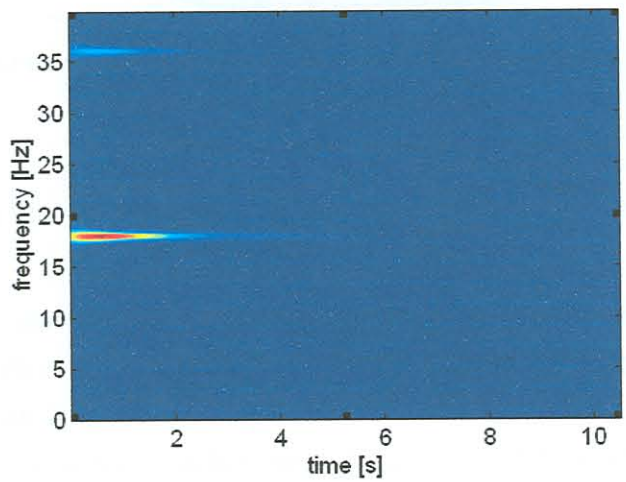

Figure 4.11: Gabor spectrogram of thrust force when workpiece is clamped skew

4.3.4 Internal disturbance - chatter

In some cases, tool chatter appeared due to tool wear effects. Chatter also caused a very irregular chip formation. Upon analysing the data, it was found that chatter cause a high vibrations at about 800 Hz, as depicted in Figure 4.12. The signal number / index in the figure refers to each new measurement. The 800 Hz peak occurred in two experiments on different machines. The effect was removed from the signals by using a digital notch filter.

4.3.5 Internal disturbance – chip formation

During all experiments, the cutting process was observed closely and notes were kept on the chip behaviour. In some cases, a very irregular formation of the chip was observed. Sometimes a very big and irregular curled chip was observed, and in other cases a very smooth behaviour was observed. Sometimes the chips seemed to 'stick' to the tool. Figure 4.13 is a smoothed plot (logarithmic scale) of the thrust force spectrum in the region influenced by chip formation. The behaviour of the chips seems to be totally random, with no connection to tool wear or any other measurable process parameter. However, the instability of chip formation increases with increasing tool wear. This behaviour can also be

seen in the recorded signals, where the force signals are dominated by the frequency related to chip formation. For a very smooth cut, a higher frequency (approx. 26 Hz) with lower amplitudes was observed. For an irregular cut, a lower frequency with higher amplitudes was observed (approx. 8 Hz). Another important region for chip formation was found to be around 15 - 20 Hz.

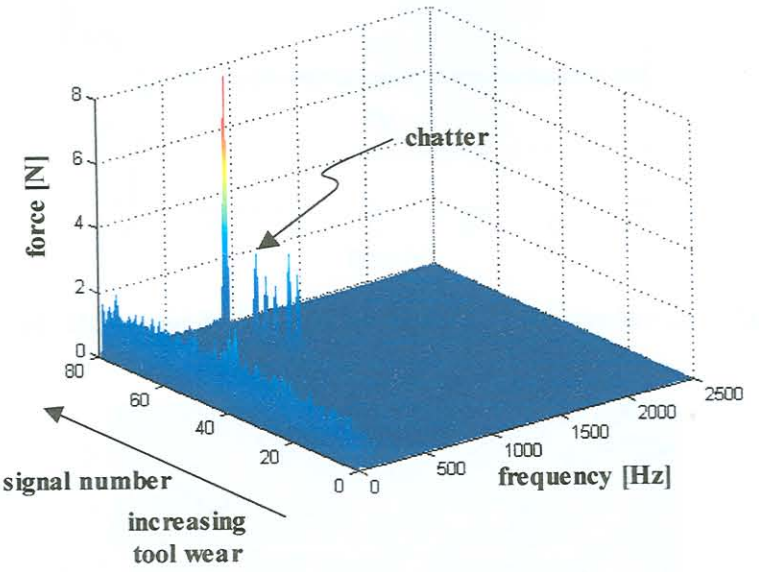

Figure 4.12: Spectra of thrust forces experiment 1

An example of a measurement where the chip suddenly changed from a smooth formation to an irregular formation with big curls is presented in Figure 4.14. A Gabor spectrogram of the thrust force reveals the frequency domain behaviour in Figure 4.15. It is clear that the dominant frequency jumps quite suddenly from 26 Hz to 8 Hz. Another example of cutting forces when the chip curl was visibly big and unstable is plotted in Figure 4.16 with its Gabor spectrogram in Figure 4.17.

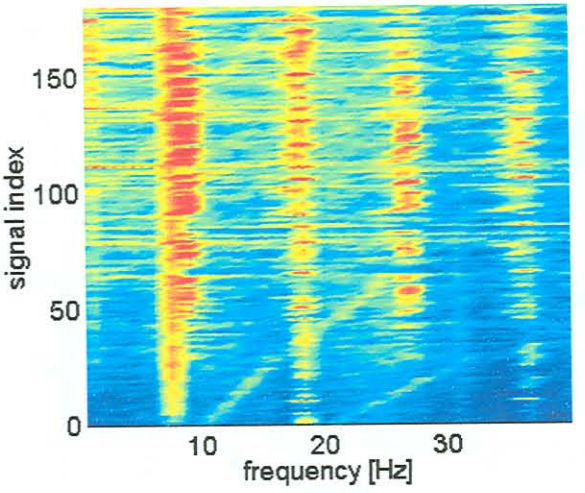

Figure 4.13: Chip formation from forces - thrust force experiment 4

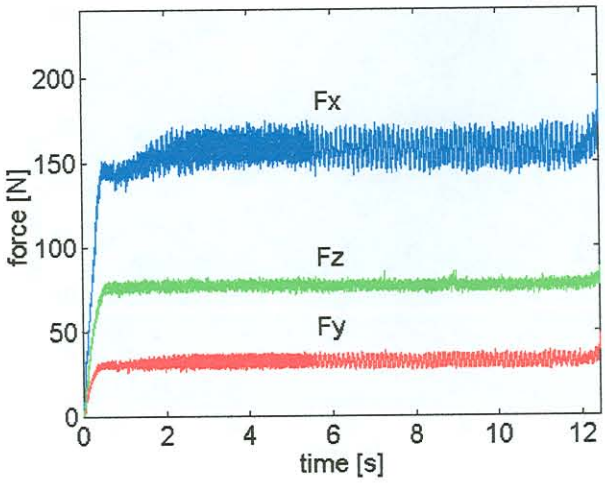

Figure 4.14: Response history of forces during irregular chip formation

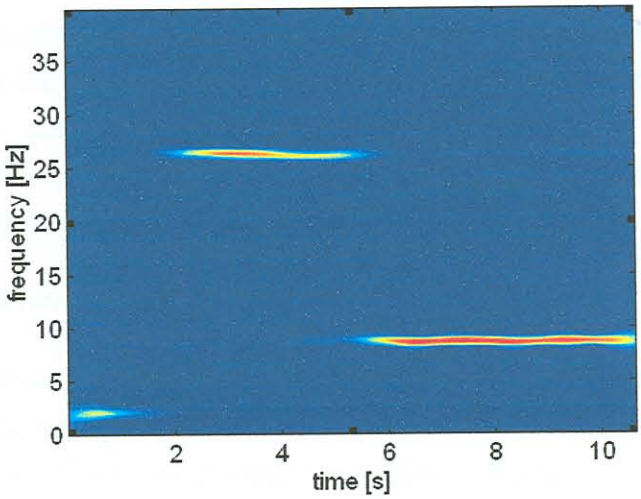

Figure 4.15: Gabor spectrogram of thrust force during irregular chip formation

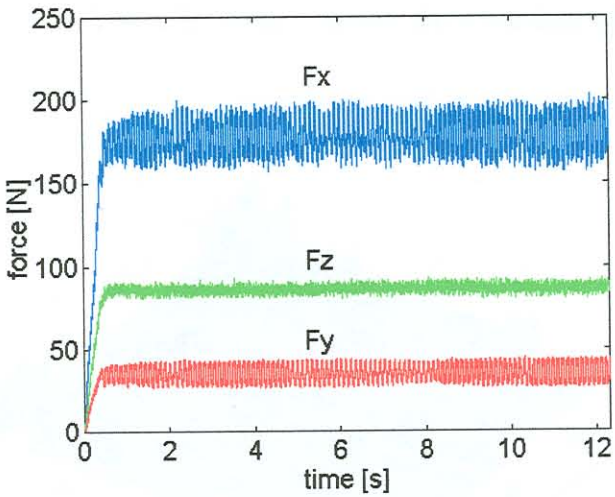

Figure 4.16: Cutting forces with big and unstable chip curl

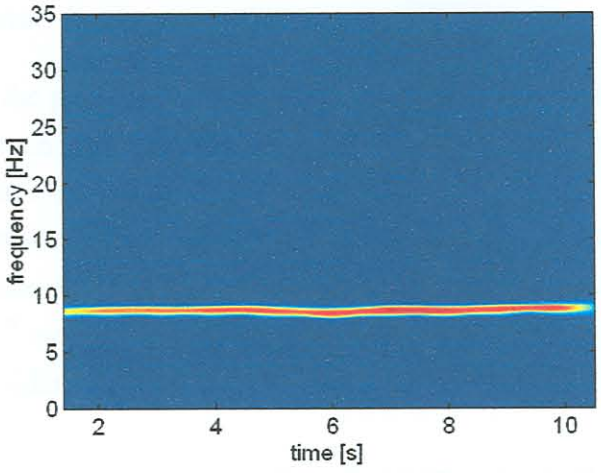

Figure 4.17: Gabor spectrogram of thrust force with big and unstable chip curl

It was concluded that time-frequency analysis can be used to monitor the behaviour of the chip, but cannot be used to enhance the performance of the tool wear monitoring system. No reliable features for wear monitoring could be derived with this technique, and the behaviour of the chip is chaotic with respect to tool wear. It is however important to identify stationary sections in the signals with the aim towards further analysis in the frequency domain (to follow).

4.3.6 External disturbance - electrical noise

Another external disturbance is that caused by the environment. Environmental disturbances are usually due to electromagnetic energy emitted from nearby machinery or even the machine under test. In this case, a 50 Hz (corresponding to the electrical transmission frequency in Germany) peak was found in the force data. The disturbance amplitude is low in the morning and grows as the day progresses. This could be the influence of nearby machinery as more machines are switched on during the day. An example from experiment 2 is shown in Figure 4.18, where data over two days is shown. The disturbance is shown in terms of volts. This effect was removed from the data with digital filtering.

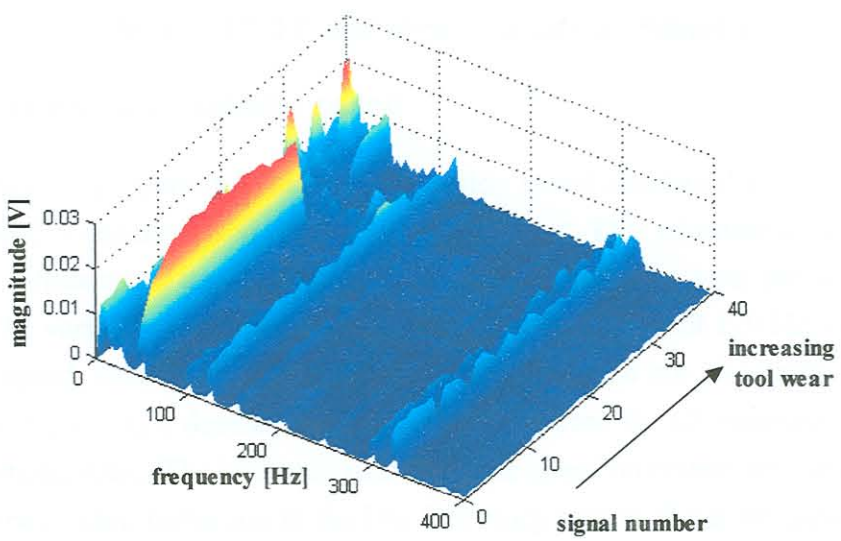

Figure 4.18: Spectrum of feed force data experiment 2

4.3.7 Internal disturbance - tool wear

An inherent disturbance to the process is of course the tool wear. With all other disturbances identified and isolated, it would be much easier to identify parameters influenced by the inherent disturbance of tool wear. As can be seen in Figure 4.19, some regions on the frequency spectrum show a definite increase with progressive tool wear. It was found by this (and previous) investigation that the frequency regions most likely to increase due to tool wear are those corresponding to the tool holder natural frequencies. In this case the 1st mode is near 1 kHz, which is the resonance frequency of the fixed dynamometer clamping a tool holder.

The overhang length of the tool holder is another important consideration when searching for wear sensitive frequencies. In the case of a dynamometer setup, there is a prescribed length (35 mm for the Kistler 9121) prescribed by the sensor calibration specifications. The stiffness, geometry and overhang length of the tool holder determines the values of the natural frequencies. Generally, it can be determined experimentally by an impact (with modal hammer) test, and verified analytically. Some authors also suggest the use of finite element modelling [97].

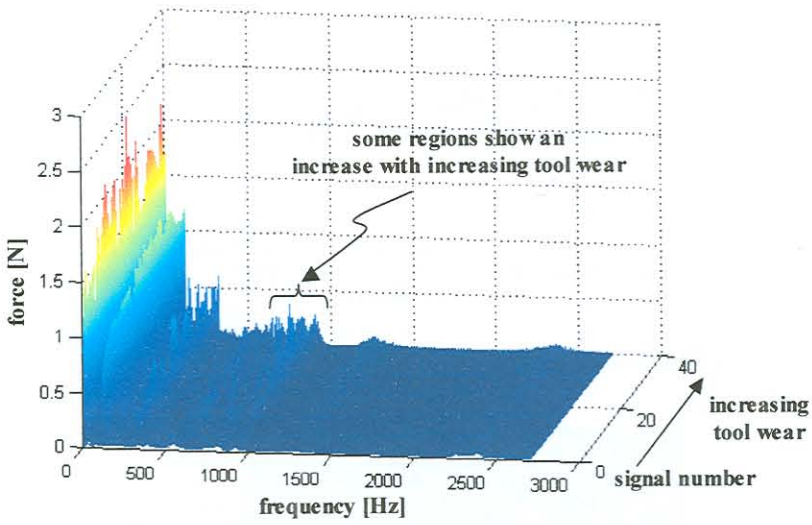

Figure 4.19: Filtered thrust forces experiment 1

4.3.8 External disturbance - spindle speed

Most CNC machines are programmed to keep the cutting speed constant during overruns. This means that the spindle speed is adjusted according to the depth of cut. This adjustment of spindle speed has a minor but notable influence on cutting test data. The results from two tests are shown in Figure 4.20 and Figure 4.21. The variation in cutting speed is clearly visible at about 120 Hz, corresponding to the spindle rotational speed. Other related frequencies in the spectrum are also influenced, but the influence is very small. Figure 4.22 depicts the thrust force spectrum for all measurements during experiment 4 on a logarithmic scale. The influence of the spindle speed on certain frequencies can be seen, as well as the influence of chip formation in the low frequency region. It can be concluded that the spindle speed does not have an influence on chip formation, because the cutting speed remains constant.

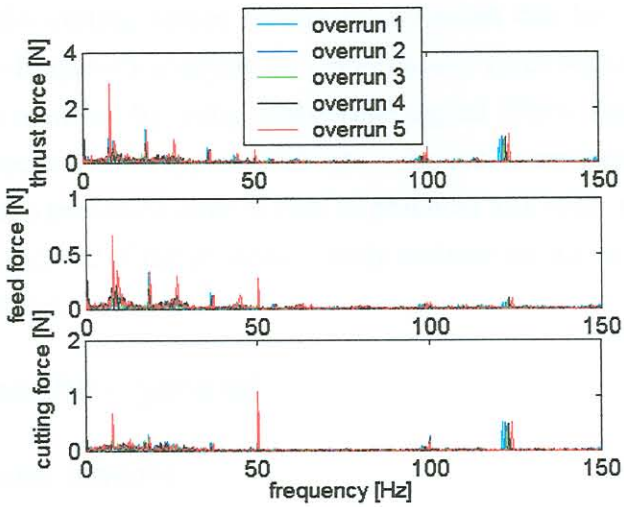

Figure 4.20: Experiment 4 piece 11 forces

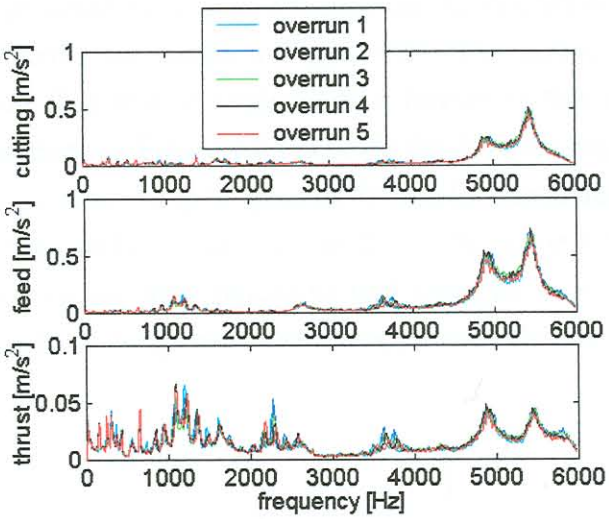

Figure 4.21: Experiment 4 piece 11 acceleration

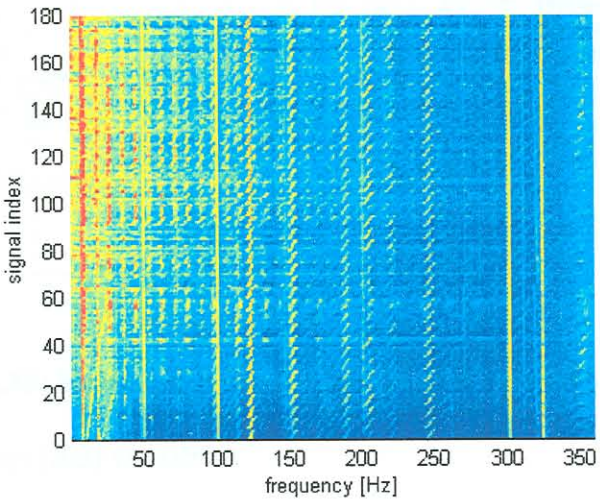

Figure 4.22: Thrust force spectrum experiment 4 (logarithmic scale)

4.3.9 Discussion

An interesting external disturbance proved to be removal of the tool insert for wear measurements. The slightly different clamping situation of the tool insert has an influence on vibration and the static and

dynamic components of the cutting forces. These disturbances can be identified with ease by frequency and / or joint time-frequency analysis of vibration and force signals. Furthermore, their influence on the signals can be removed by using appropriate digital filters. Further investigations revealed that the identified disturbances had no apparent effect on the tool wear growth rate. It should be kept in mind that the analysis results presented here is vital to practical tool wear monitoring. A generic monitoring approach can only succeed if the process is fully understood and the effects of the various disturbances are compensated for.

4.4 Experimental results - general

4.4.1 Temperature measurements

During experiment 1, temperature measurements were taken to determine if external temperatures (those not inherent to the process) have any influence on the operation. The results of temperature measurements from experiment 1 are shown in Figure 4.23. The temperature measurements revealed some interesting correlations that will be explored in a further section using Self Organising Maps (SOMs). The vertical dotted lines on Figure 4.23 indicate the different days over which the experiment was conducted. The start of each new day is apparent from a low temperature that increases as the day progresses. The room and the machine temperatures follow the same trends. The temperature of the workpiece after machining increase with increasing tool wear, as expected. However, investigations showed that the room and machine temperature had no apparent influence on the rate of tool wear.

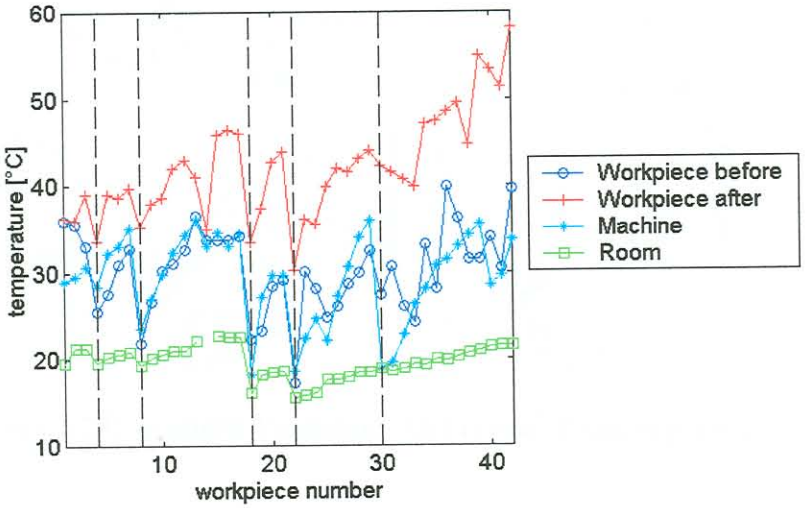

Figure 4.23: Results of temperature measurements experiment 1

4.4.2 Acoustic Emission (AE) results

The results of the AE recordings during experiment 1 are shown in Figure 4.24 (the solid lines are 3rd order polynomial fits of the scattered data). The AE signals were treated with four different analysis methods, all of which eventually displayed the same tendencies. It can be seen that the AE energy starts at a high level, and then decreases to a minimum at about 0.04 mm flank wear. Then it starts to increase again and reaches the highest levels towards the end of the experiment. This result corresponds to that of a very recent study by Tönshoff *et al.* [220]. They provide the following explanation:

"A tool without flank wear generates high AE amplitudes from the sharp-edged tool and the lower damping rate of the tool-workpiece system. With increasing flank wear, the damping rate grows and the generated AE amplitude of the process decreases to a lower bound. If the mechanical and thermal load during machining increases in combination with the appearance of white layers and tempered zones, a continuous increase of the amplitude can be recorded." The same result was also found with different machining parameters.

It can thus be concluded that AE can be used to identify the moment during hard turning where mechanical and thermal loads start to increase. An added result of this case study to that of Tönshoff *et al.* is the fact that the AErms, directly recorded from the rms sensor output without filtering, can also be used to trend the AE energy. The AErms is much easier to record and process compared to the real-time AE signal that requires a sampling rate above 400kHz. Parameters calculated from frequency and time domain analysis did not show significant improvement of the results compared to the AErms. A difficulty with the AE and AErms signal is the fact that it exhibits a lot of variance, and is therefore prone to create false alarms in a production environment. It was decided to omit monitoring of AE during further experiments.

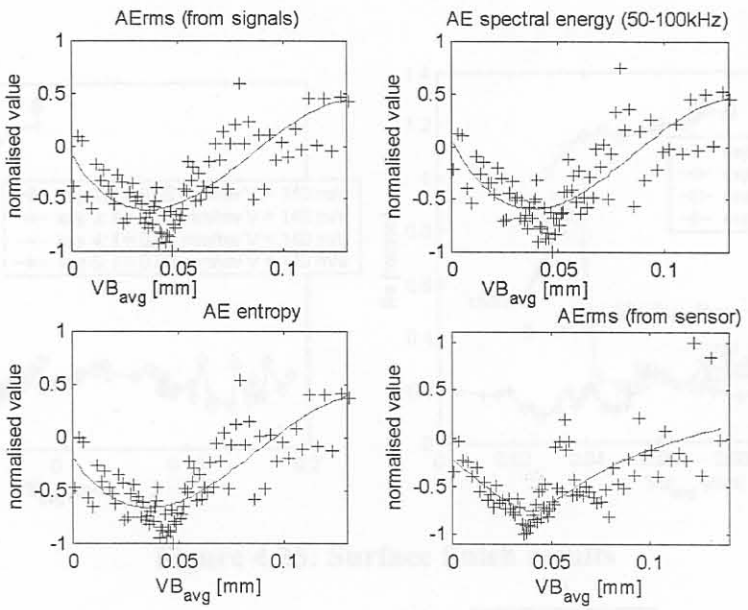

Figure 4.24: Acoustic Emission (AE) results from experiment 1

4.4.3 Surface finish and diameter

Measurements of the surface roughness and diameter of the machined workpieces revealed some interesting facts. It was found that there is not a very clear relationship between the tool wear and the workpiece geometry. The reader is referred to Appendix I for notes on surface roughness measurement and analysis. As general rule the following behaviour is expected:

- Surface roughness will increase initially, then reach a maximum, then decrease suddenly and then start to increase again towards the end of the tool life. This is caused by micro-breakage of the cut-

ting edge after a considerable length of cut. The breakage caused the creation of a new, sharper cutting edge. This process can repeat a few times, after which the edge will deteriorate until complete failure. Thus, more unstable behaviour can be expected towards the end of the tool life.

- The diameter of the workpieces after machining will increase with increasing tool wear, due to the fact that tool material is removed from the cutting edge.

The behaviour of the surface roughness, displayed as the measured Ra values with respect to tool wear in Figure 4.25 (grouped into experiments with the same and different machining parameters), seemed to follow the above-mentioned assumptions. However, the workpiece diameter measurements, shown in Figure 4.26, did not clearly exhibit the expected behaviour. This was due to the fact that the tool was regularly removed from the holder for wear measurements, and it was concluded that this is also responsible for the large variation in the surface roughness values. Although the surface roughness generally increases with increasing tool wear, the relationship is very complex and difficult to generalise. The surface finish of hard turned components can be improved by a secondary process called roller burnishing. However, worn tools will cause weaknesses in the workpiece subsurface and therefore tool wear monitoring is still very important. From the figures it is obvious that it will be extremely difficult to estimate the degree of wear using surface finish information only (and vice versa).

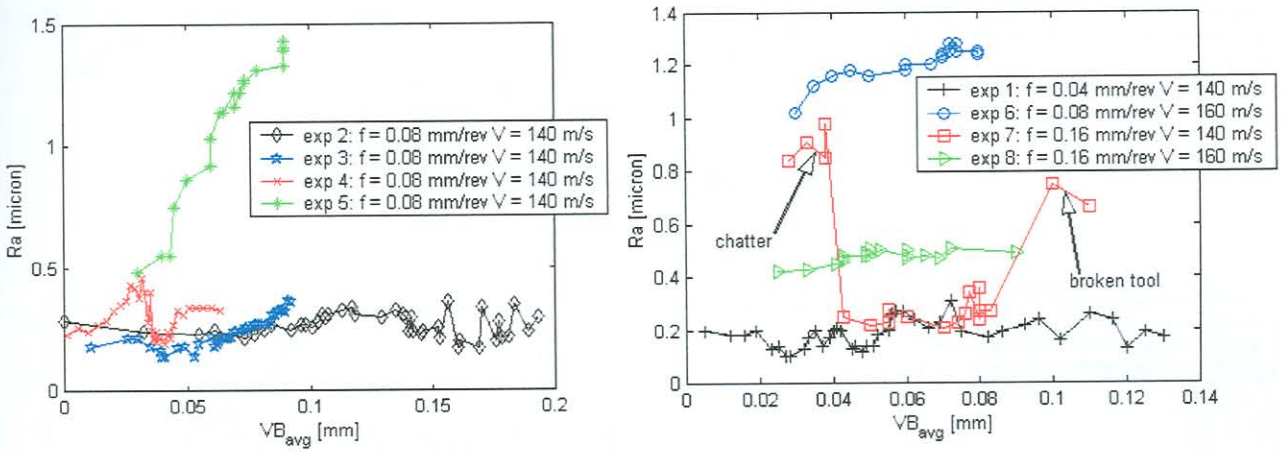

Figure 4.25: Surface finish results

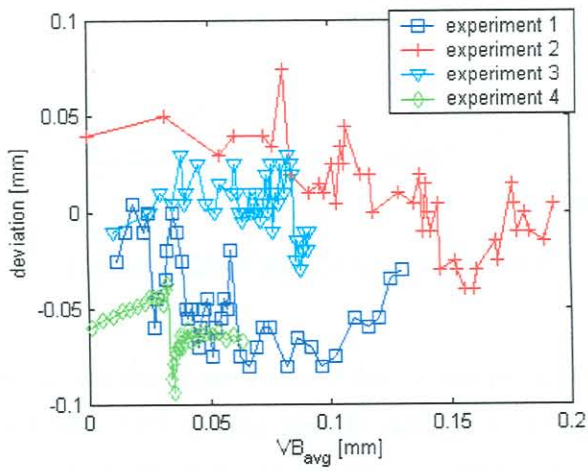

Figure 4.26: Workpiece diameter deviation

4.4.4 Tool wear

The area of the flank wear for the different experiments is plotted in Figure 4.27, with the volume of the crater wear in Figure 4.28. A very interesting fact is revealed in these figures: Experiments 2 and 3 were conducted with the exact same machining parameters, tool type and workpieces, but the wear behaviour is completely different. The only difference between the two experiments is the number of engagement impacts on the tool, which were more during experiment 2. Also, the time delays between overruns were a little longer during experiment 3. Thus, the number of engagements and cool-down time allowed between overruns is an important consideration when considering the life of hard turning tools. A slight difference in quality of the tool coating and workpiece material could also have an influence on the tool life, but the margin of difference is very small.

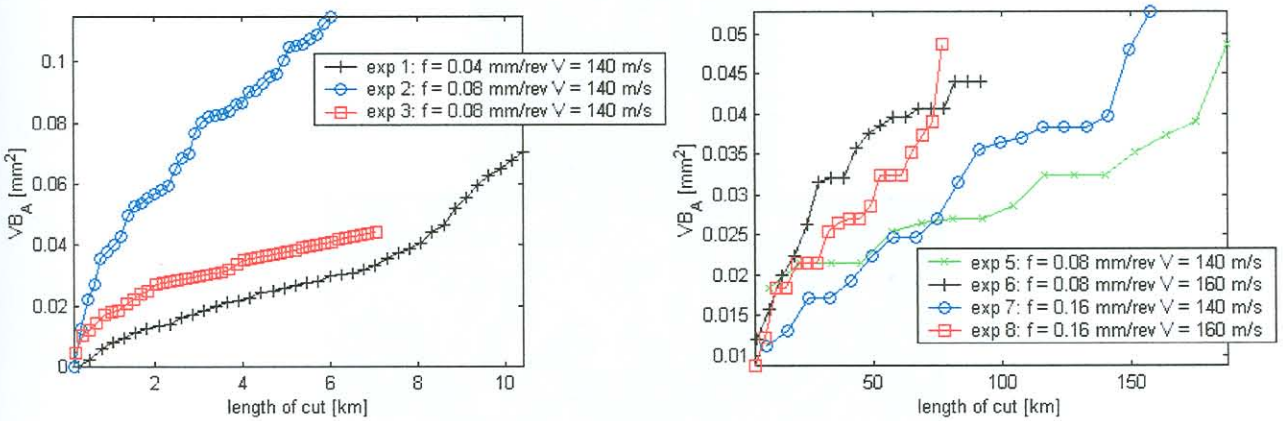

Figure 4.27: Area of flank wear

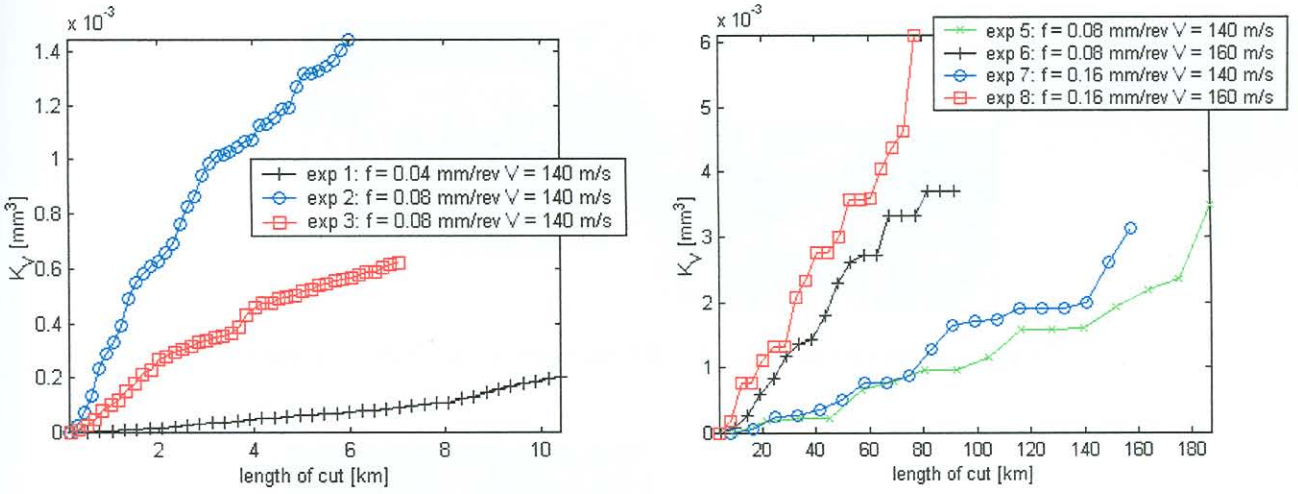

Figure 4.28: Volume of crater wear

The growth of tool wear was slower for experiment 1 due to the lower feed rate. The tool wear is also influenced by the higher feed rates and cutting speeds used in experiments 7-8. The machining parameters for experiment 5 are exactly the same as during experiments 1-4 (besides the workpiece hardness which is slightly different) but the rate of tool wear is much slower.

Scanning Electron Microscope (SEM) pictures of the cutting edges from experiments 1-3 are shown in Figure 4.29. The big differences in the wear geometries of flank and crater wear from the different experiments are clear from these images, especially when comparing the crater wear which was formed under the exact same machining parameters (experiments 2 and 3). Further pictures of the wear on the tools used in experiments 7 and 8 are shown in Figure 4.30 and Figure 4.31, respectively. These pictures were taken with an optical microscope with a digital camera attachment. The geometries of the flank and crater wear in each case can be compared, and it is clear that the particular geometry is unique in each case. Both the flank and crater wear have an influence on the stability of the process. The influence of the wear geometry on the parameters for wear monitoring will be discussed in a following section.

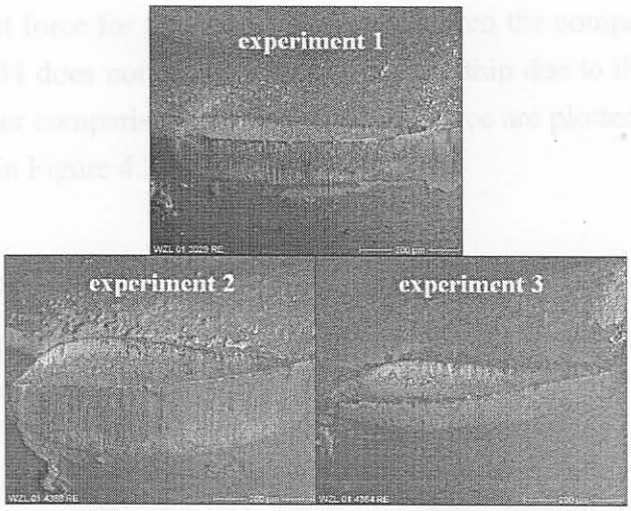

Figure 4.29: SEM pictures of cutting edges

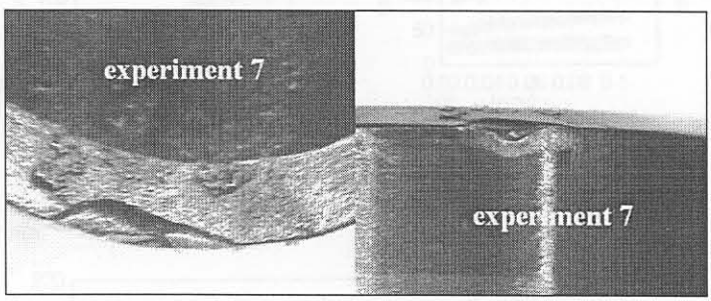

Figure 4.30: Crater wear and flank wear insert experiment 7

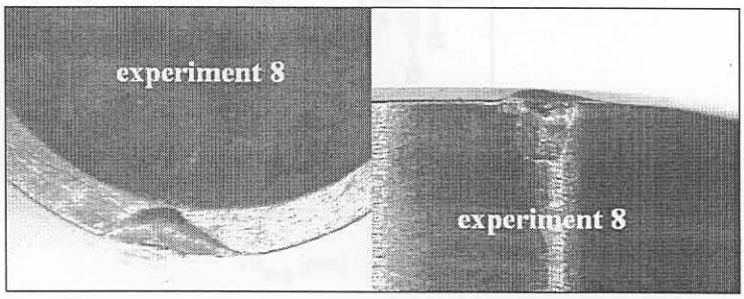

Figure 4.31: Crater wear and flank wear insert experiment 8

4.4.5 Static forces

The static cutting forces are commonly used as tool wear monitoring features. The results of this and previous studies show that the thrust force is the most reliable static force direction to monitor tool wear during hard turning. However, the static parameters alone are not sufficient for a reliable monitoring system. This is due to the fact that they display much variation and are influenced by the disturbances described earlier. The behaviour of the static forces is depicted in Figure 4.32. Apart from changes in machining parameters, there were two major influences on the static forces. The first influence is the removal of the tool for wear measurement. The second major influence seems to be the 3-D geometry of the tool wear itself. When referring to a direct comparison of the static cutting forces, such as the thrust forces in Figure 4.33, it can be seen that there is not a consistent relationship between VBavg and the thrust force for the four experiments. Even the comparison of different machining conditions in Figure 4.34 does not reveal a simple relationship due to the large degree of variance in the measurements. Further comparisons of the static feed force are plotted in Figure 4.35 and Figure 4.36, and the cutting force in Figure 4.37 and Figure 4.38.

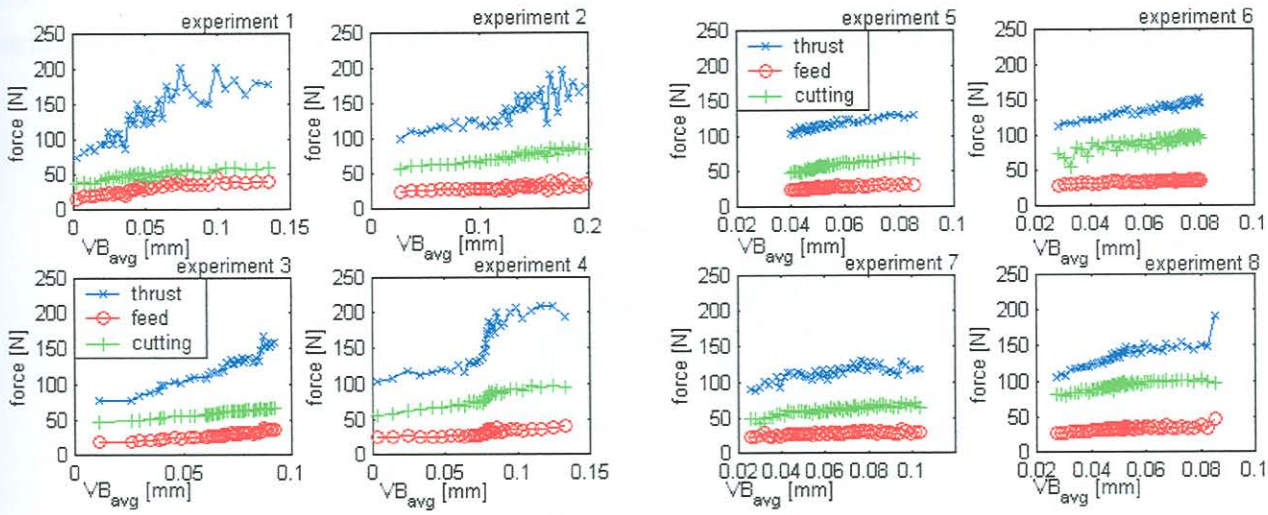

Figure 4.32: Static forces

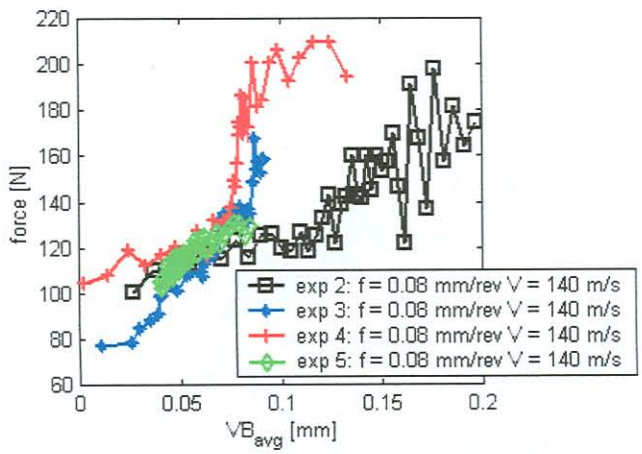

Figure 4.33: Static thrust forces (1)

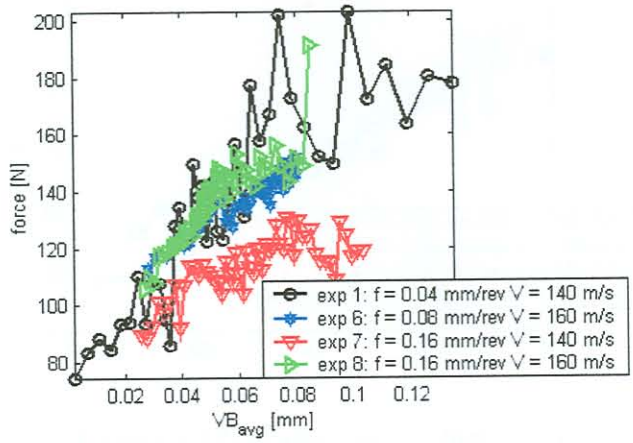

Figure 4.34: Static thrust forces (2)

Due to the fact that all controllable parameters during experiments 2, 3 and 4 remained the same, it can be postulated that the shape of the crater can cause the process to be more unstable and thus cause more random variations in the static (and dynamic, discussed in the following section) forces. The variation in the static cutting forces creates major difficulties from a modelling point of view.

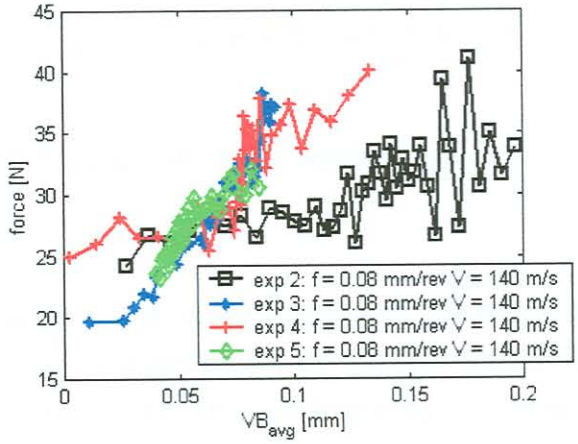

Figure 4.35: Static feed forces (1)

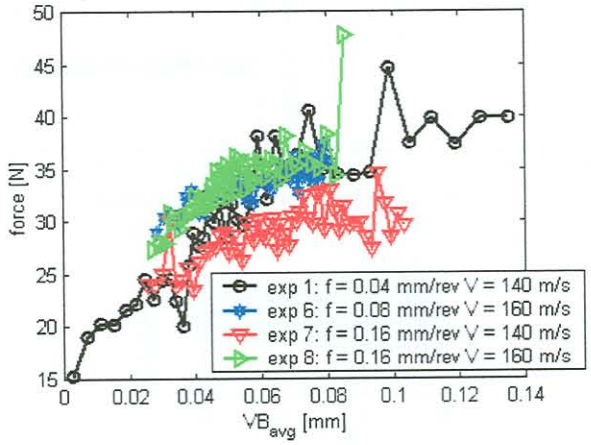

Figure 4.36: Static feed forces (2)

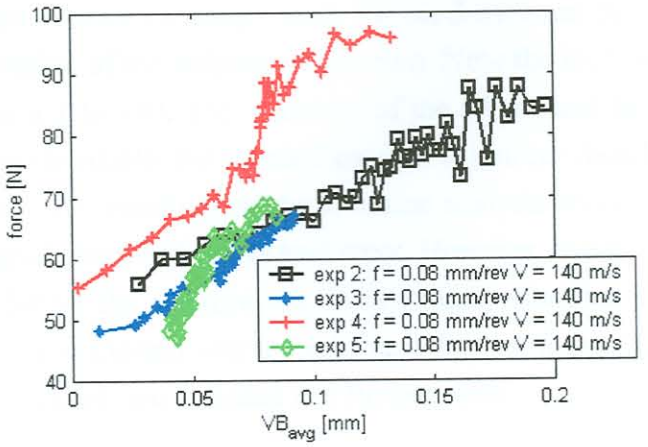

Figure 4.37: Static cutting forces (1)

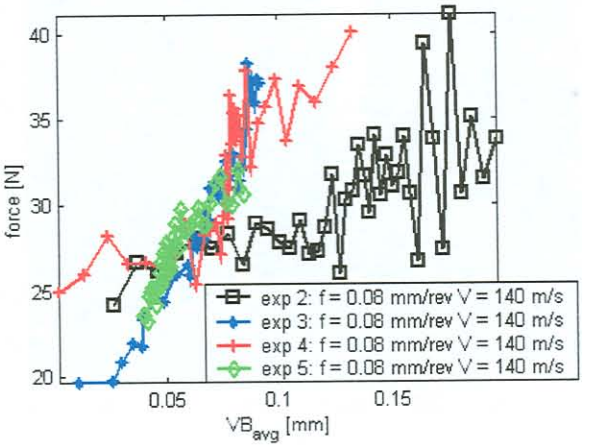

Figure 4.38: Static cutting forces (2)

4.4.6 Vibration analysis

A typical response history of acceleration during experiment 2 is shown in Figure 4.39. It can be seen that the vibration levels are fairly low, especially in the thrust direction. The basic method of analysing vibration signals in TCM is to check the vibration frequency spectrum for regions sensitive to tool wear.

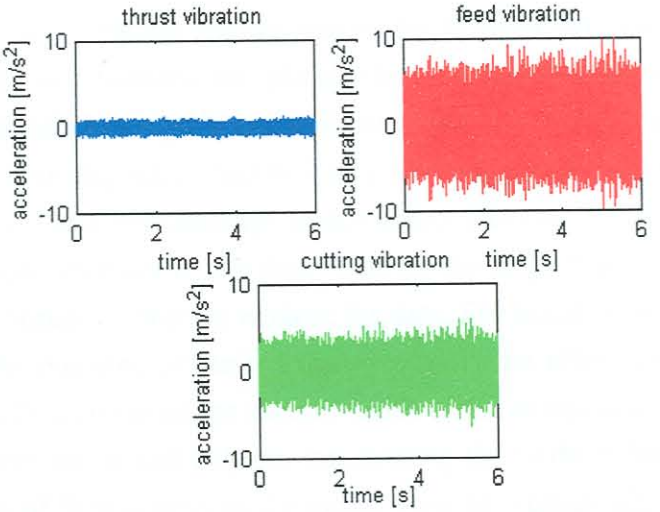

Figure 4.39: Typical acceleration signals experiment 2

Figure 4.40 depicts the thrust vibration measurements for the 5 overruns per workpiece during experiment 4 in a wear sensitive region of the frequency spectrum. Note the increase in vibration amplitudes at 1.2 kHz from measurement 1 to 180. The influence of the adjustment in cutting speed (due to decreasing workpiece diameter) is visible, but is small enough to ignore when looking at spectral energy values in a certain bandwidth. The results from the vibration analysis revealed that certain features derived from the vibration signals are sensitive to tool wear. However, it was difficult to determine features that were consistent for all the experiments. Furthermore, vibration is also sensitive to disturbances, and it is often difficult to explain why a particular vibration feature is influenced by tool wear. More results of the vibration signals are included in a further section.

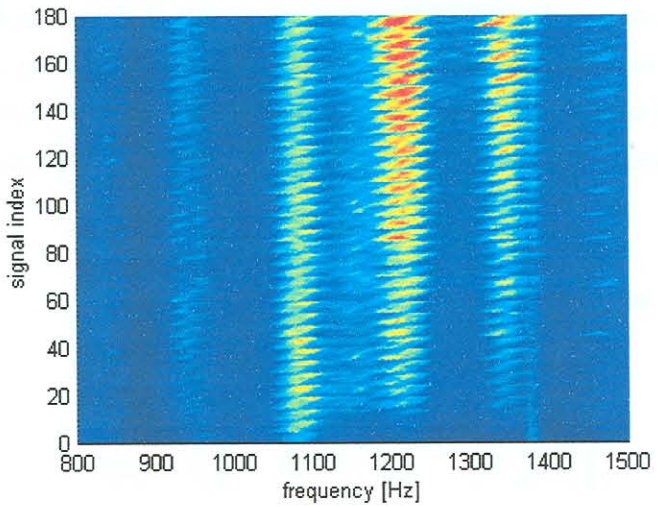

Figure 4.40: Thrust vibration spectra experiment 4 (linear scale)

4.5 Experimental results - correlation analysis with SOMs

4.5.1 Purpose of SOM analyses

To investigate the effect of all the different variables described in the previous section, several Self-Organising Map (SOM) analyses were conducted. The SOM is an unsupervised NN, also known as a Kohonen map, after their inventor [221], and is rapidly becoming a well-known tool for data exploration. The SOM automatically arranges multi-dimensional observation data on a two dimensional grid of neurons where similar observations are placed close to one another and dissimilar ones further away. In this way, hidden relationships in multi-dimensional data can be identified with a SOM analysis. In the case of the hard turning experiments, it was necessary to identify possible relationships in all the measured parameters. These relationships or correlations in the sensor information can also assist in the identification of disturbances in the data. Due to the large amount of sensory information, a SOM analysis is an appropriate method to explore the data. For instance, it was necessary to determine if the temperature of the machine or its surroundings have an effect on the process performance. Furthermore, the effect of tool wear on the surface finish of the components can also be investigated in this way. A detailed formulation and help on interpreting the SOM is included in Appendix H. For help on the interpretation of SOMs, refer to the recent work by Vesanto [222].

4.5.2 Results

A SOM analysis with data from experiment 1 is shown in Figure 4.41. The SOM reveals the relationship between surface finish (Ra), tool flank wear (VB), entropy (refer to Appendix F) of the Acoustic Emission (AE) signal, the static thrust force (Fz) and the temperature of the machine. From the SOM analyses it can be concluded that Ra does not degrade linearly with tool wear. It rather seems to reach a maximum value during medium wear conditions, and then decrease again. However, VB > 0.1 mm generally induces the formation of white layers, and should be avoided. Other observations are that the machine temperature has no influence on the workpiece surface finish, and that the static thrust force correlates well with tool wear. The results from the AE signal shows that AE reaches a minimum value at about 0.05 mm flank wear, and then start to increase again towards the end of the tool life, as shown in Figure 4.24. A sharp edged tool will cause high values of AE. During the normal worn phase of the tool, there is more damping present in the process, which cause the AE to decrease. During the final stage of the tool's lifetime, very high temperatures in the deformation zones and the onset of white layers cause an increase of AE.

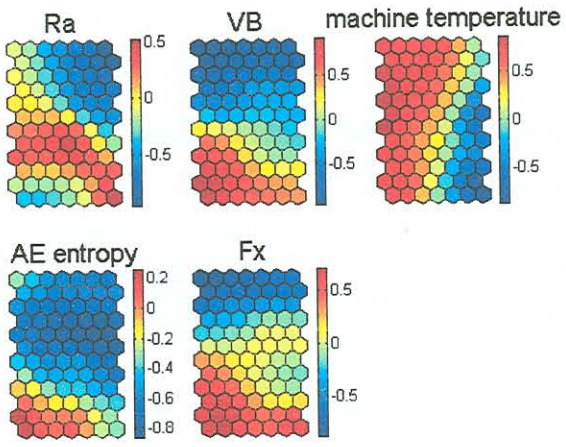

Figure 4.41: SOM analysis experiment 1 (1)

The result of a SOM analysis involving all the significant parameters from experiment 1 is shown in Figure 4.42. The SOM analysis basically confirms what was mentioned in the previous paragraphs dealing with experiment 1. From this analysis, the influence of (for example) tool wear on the other measured parameters can be derived. These influences are summarised in Table 4.5.

Table 4.5: Influence of VB on other variables:

	VB low	**VB high**
Surface Rz	Lower	Higher
Surface Ra	Lower	Higher
Workpiece diameter	Low and high values	More high values
Temp WP after	Towards lower values	Towards higher values

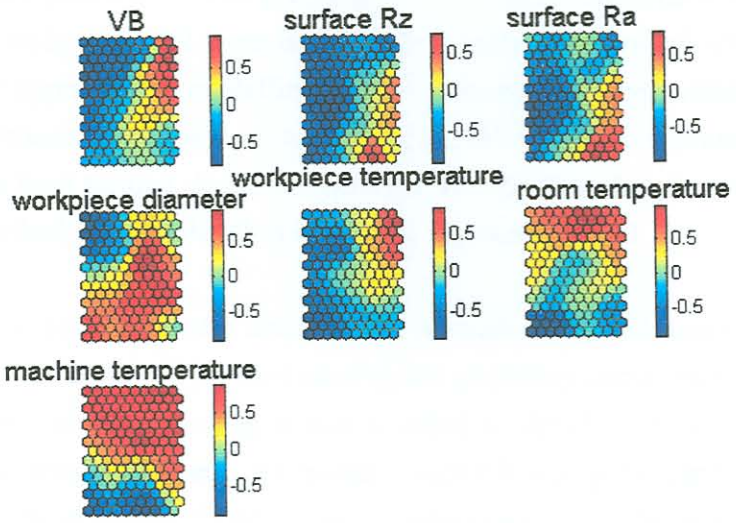

Figure 4.42: SOM analysis experiment 1 (2)

Furthermore, the influence of the machine temperature on the other parameters can also be derived. These results are summarised in Table 4.6.

Table 4.6: Influence of machine temperature on other variables:

	Temperature Machine low	Temperature Machine higher
Surface Rz	No apparent influence	No apparent influence
Surface Ra	No apparent influence	No apparent influence
Workpiece diameter	Show generally high values	High and low values

Another important conclusion from the SOM analysis is that the workpiece diameter is not influenced much by tool wear or the temperatures. Some recommendations resulting from this analysis were that the measurements of the workpiece and room temperatures be omitted for further experiments. The room temperature does not play a significant role, and the workpiece temperatures are difficult to measure accurately because the workpieces cool down very quickly after machining. The workpiece temperatures are also more governed by the time delay between two overruns than tool wear. Signal features were also investigated for sensitivity towards tool wear with SOM analyses.

4.6 AI approach for wear monitoring

4.6.1 Introduction

In order to establish a reliable method for monitoring the tool wear during hard turning, an appropriate wear model is required. During the course of this research many different types of modelling methods were investigated for their feasibility towards hard turning. Analytical and empirical methods have been developed through the years that can model many different machining operations. Analytical models are often deemed as too complex to be practical for a production environment. On the other hand, recently developed analytical and combined models can accurately model the behaviour of quite

complex tool / workpiece geometries. The problem with analytical methods is that they cannot model the behaviour of worn tools, and tool wear is a fact that cannot be avoided with present technology. Recently, a mechanistic approach for modelling worn tool forces appeared, which is probably the most novel combination approach developed up to date [223]. However, implementation of the method proved unsuccessful for hard turning due to some of the assumptions that do not apply to hard turning operations. This is described in more detail in Chapter 6 and Appendix G.

Hard turning experiments revealed that a combination of crater and flank wear govern the stability of the process. A worn tool force model for hard turning not including crater wear will not succeed. Considering this experience with hard turning it was decided to develop an Artificial Intelligence (AI) method with NNs to monitor tool wear. AI models resemble non-parametric empirical models, but have some advantages above conventional empirical equations. With the aim to ultimately estimate tool wear on-line with force measurements, it was decided to develop a NN monitoring strategy that utilises sets of static and dynamic NNs. The advantages of various NNs paradigms above other methods were described in Chapter 3. However, before the AI monitoring method can be described, certain signal features should be identified by means of signal processing and feature selection.

4.6.2 Signal processing

The usual signal processing procedure for TCM is to generate many signal features and then apply some kind of feature selection strategy to identify features that are most sensitive to tool wear. There are four domains from which features from sensor signals can be generated:

1. Statistical analysis
2. Time domain analysis
3. Frequency domain analysis
4. Joint time-frequency analysis (*e.g.* spectrograms and wavelet analysis)

Before choosing any of the domains for feature extraction, the following critical questions should be considered:

- Can the signal be approximated as stationary?
- Is a localisation of events in the time series important?

Signals taken from a cutting process will rarely be stationary, and hence simple time-frequency analyses with spectrograms are always necessary to identify the most stationary parts of the signal for frequency domain analysis (refer to Section 4.3). Investigations revealed the force signals are fairly stationary above about 50 Hz. In the lower frequency range, unstable chip formation causes chaotic frequency shifts. The type of chip that forms is governed by the severity of wear on the cutting edge, and there is no apparent 'reverse' effect. For the purpose of tool wear monitoring, a localisation of an event in the time series is of no importance. For monitoring tool breakage or other events, an accurate localisation could be of more importance. Therefore, for the purpose of a wear monitoring strategy for hard turning, time-frequency analysis was only conducted to investigate the general dynamic behaviour of the signals. No signal features were extracted from the time-frequency analysis.

The static components of the force signals are often used for TCM purposes, because static forces increase due to increasing friction between the tool and workpiece when wear is present. The static component is the mean of the force signal. The mean value of a signal *s(t)* over an interval T is:

$$\bar{s} = \frac{\int_0^T s(t)\,dt}{T} \tag{4.3}$$

The dynamic component of the force signal contains very useful information about the tool wear as well. The reason is because tool wear causes increasing vibration amplitudes in certain frequency ranges due to the larger frictional forces when the tool is worn. Previous research has suggested four possibilities from dynamic analyses that could be used to monitor tool wear:

1. Response at the natural frequencies of the tool holder.
2. Frequencies related to chip formation (*e.g.* chip serration and chip curl frequencies).
3. Natural frequencies of the dynamometer.
4. Vibration frequency of the tool insert when fixed in the tool holder.

Only option 1 is a practical possibility, especially when considering an industrial implementation of the TCMS. Investigations of option 2 did not reveal useful information, and option 3 is dependant on the presence of a dynamometer. Option 4 is subject to disturbance due to removal of the insert. Examples of FFTs of the force signals are shown in Figure 4.43. It is possible to identify certain frequency ranges in the FFT that are sensitive to tool wear, and the energy in such a range can be used as a signal feature with:

$$\psi_s^2 = \int_{fl}^{fh} S_s(f)\,df \tag{4.4}$$

where $S_s(f)$ is the one-sided Power Spectral Density (PSD) function of the signal and *fl* and *fh* chosen to reflect the energy in the regions of interest. The values of *fl* and *fh* should be chosen to correspond with a frequency range that will be sensitive to tool wear, and must be independent of the type of the workpiece and machine type. Investigating the tool holder response with the different experiments identified such a range between 1.20 – 1.25 kHz. This range is a natural frequency of the clamped tool holder. Figure 4.44 shows the result of the vibration (from accelerometer) energy in this range with respect to tool wear for one of the experiments. Though this feature is better measured with the accelerometer (high frequencies generate high acceleration levels), it can be extracted from the force signals as well (which is more related to displacement and hence lower amplitudes). However, to simplify an industrial implementation, it was decided to extract all the features for the method from the force signals only, and hence only one sensor would be required.

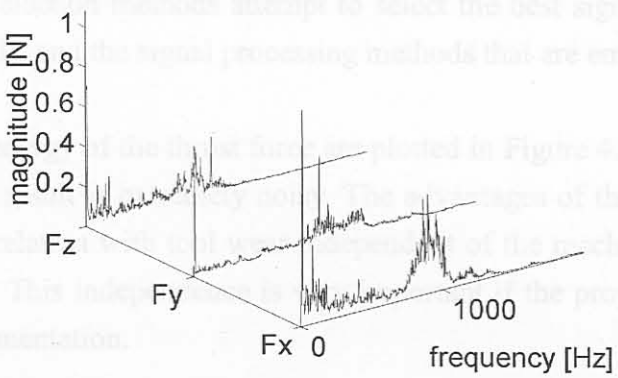

Figure 4.43: FFTs of force signals

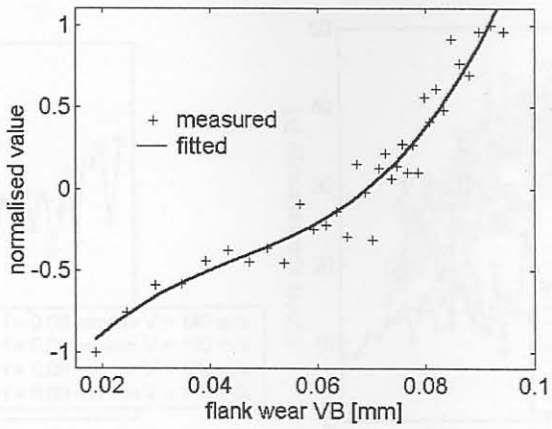

Figure 4.44: Vibration energy in the 1.20 – 1.25 kHz range (normalised)

Further signal features were generated by means of time domain and statistical analysis, but none revealed a consistent correlation with tool wear for all the experiments (typical features that were tested for feasibility are described in Section 5.6.3). Hence, based on linear correlation analyses between tool wear (crater and flank) and the various signal features, the following features were used as inputs to the NN that showed the best correlation with wear:

- static thrust, feed and cutting force (*Fx*, *Fy* and *Fz*)
- dynamic energy around the natural frequency (1.20 – 1.25 kHz) of the tool holder in the thrust force direction (*Fxd*)

These four features showed consistently increasing trends with tool wear for all the experiments (as shown previously). Linear or exponential models relating the static cutting forces with feed, speed, depth of cut and tool wear could be constructed. Such models could assist in selecting one of the static cutting forces as a feature for wear monitoring through a sensitivity analysis. Consequently a single static force component could be chosen for wear monitoring. However, for the purpose of this research, the route of automated feature selection is more appropriate. The reason for this choice is the fact that not enough data can always be gathered to construct and verify such models (also refer Chapter 2), especially if typical shop floor conditions are to be considered (refer for example to Chapter 4). Generally, features for NN models are selected through automated procedures such as correlation analyses and not through empirical verification models (there is also no need for NNs if such models are available or easily constructed). For this case study, the four features listed above were chosen because they displayed the best correlation with tool wear throughout the range of conditions investigated. Automated feature selection methods attempt to select the best signal features for NN models using the experimental results and the signal processing methods that are employed.

The results of the spectral energy of the thrust force are plotted in Figure 4.45. Once again, an increasing trend is visible but the result is extremely noisy. The advantages of the selected four features are that they showed good correlation with tool wear independent of the machine, workpiece, tool holder and machining parameters. This independence is very important if the proposed method is to be considered for industrial implementation.

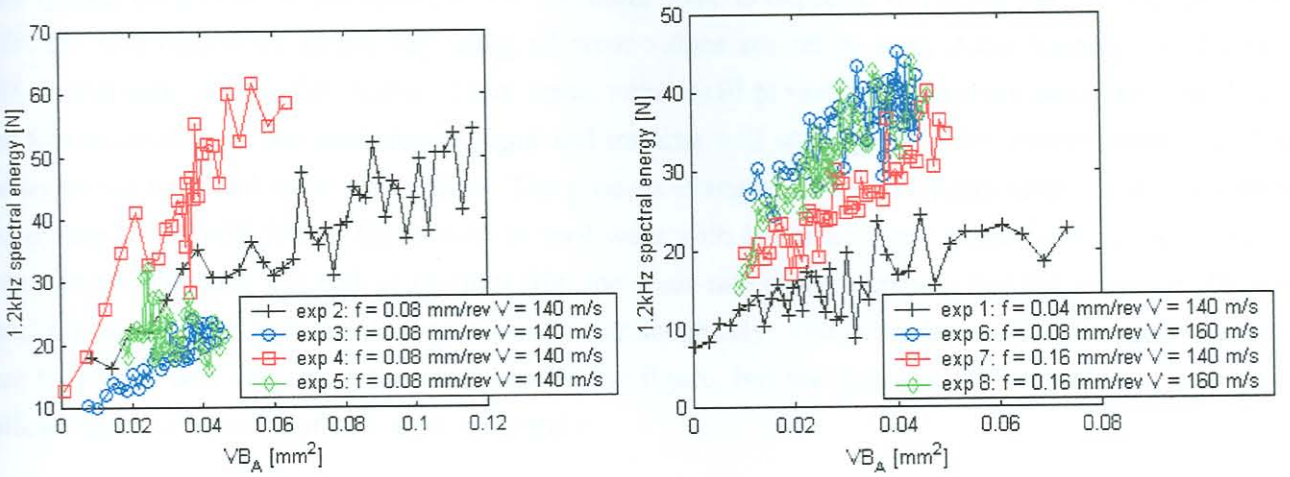

Figure 4.45: Spectral energy for thrust force

4.6.3 Formulation of method

The monitoring strategy was formulated in such a way that it utilises a combination of static and dynamic NNs. The advantages of using dynamic NNs for TCM were discussed in Chapter 3. In this research, a unique combination of static and dynamic NNs is proposed and will be shown to outperform other NN paradigms. The static NNs are trained to each model a particular feature with the flank wear, crater wear, cutting speed and feed rate as inputs. Early stopping is used to ensure generalised training, and separate training, validation and testing data sets were used (by means of cross-training and validation). The static networks each consist of a three-layer FF network, with ten sigmoid neurons in the middle layer and a tansig neuron in the output layer.

The dynamic NNs are trained on-line to estimate the wear values. The training target of the dynamic network is to minimise the difference between on-line force measurements and the output of the static networks. The advantage of this method is the fact that any development of wear can be followed on-line. The dynamic NNs use the previous three estimated wear values to estimate the next value of tool wear. This creates the ability to estimate an accurate value for the tool wear even if the training does not converge within the specified tolerance. This may happen if there was a problem with the measurement or disturbances in the signal. The behaviour of the dynamic NNs is thus to follow the curve or line of the present wear estimations, with the help of the on-line measurements and static networks. However, the method is able to generalise if errors or random disturbances occur. Another advantage is the fact that the dynamic NNs are able to follow the unique development of wear on the tool insert through on-line training. Thus, the dynamic NNs have delay and recurrent characteristics.

The method utilises sets of inner and outer steps or time-increments. The inner steps are training steps of the dynamic NNs to achieve a specified convergence. During the inner steps, the tool wear is assumed constant and the combined NNs attempt to estimate this value. When this is achieved, an outer step is taken, and in this case it is an incremental step in the tool wear. A schematic representation of the method is shown in Figure 4.46. There are two dynamic NNs: One to follow flank wear (DN_1) and the other to follow the growth of crater wear (DN_2).

The typical behaviour of the dynamic NN for flank wear is depicted in Figure 4.47 (to be read from left/right and up/down). In the beginning all wear values are set to zero. After training the dynamic NN, it will estimate the first value of tool wear, which will probably not be very accurate. It will then use this estimation in the next step as input and training will start again. After convergence, it will be closer to the true tool wear than before. The process is repeated and normally after a few outer steps the dynamic NN will follow the growth of tool wear with better accuracy (especially in the "regular" wear stage). Towards the end of the tool life, the wear rate often increases but the dynamic NN will react on this and again follow the growth of wear accurately. The advantage is that the growth of the true tool wear will vary from the ideal case in the figure, but the dynamic NN will always attempt to follow any development of tool wear accurately.

It is obvious that the dynamic NN will become more accurate if the outer steps are taken as close as possible to one another. An outer step is taken each time a new force measurement becomes available. This is advantageous for on-line applications, because a measurement can be taken during each over-run, and hence there is enough data to keep the outer steps very close to one another.

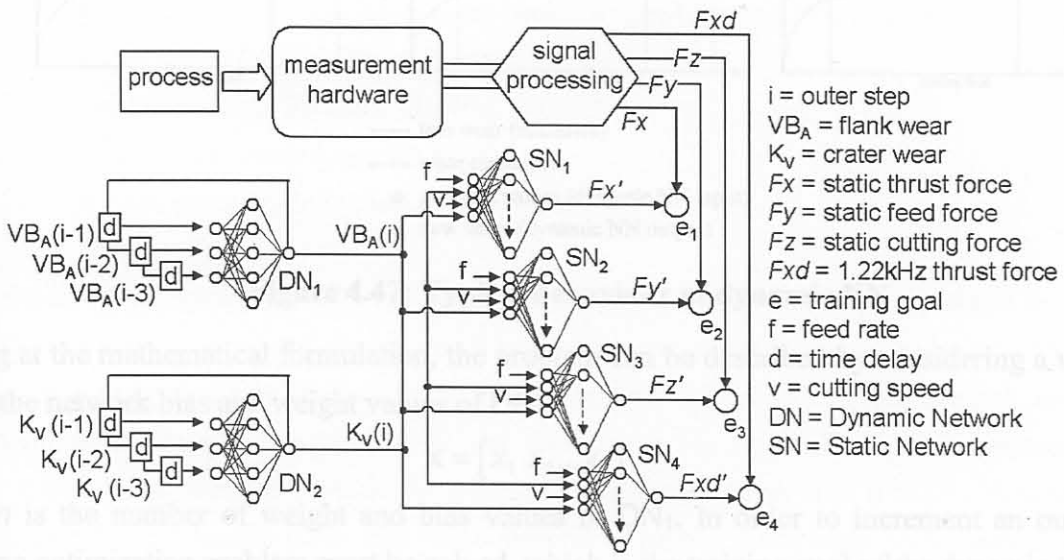

Figure 4.46: Schematic representation of monitoring method

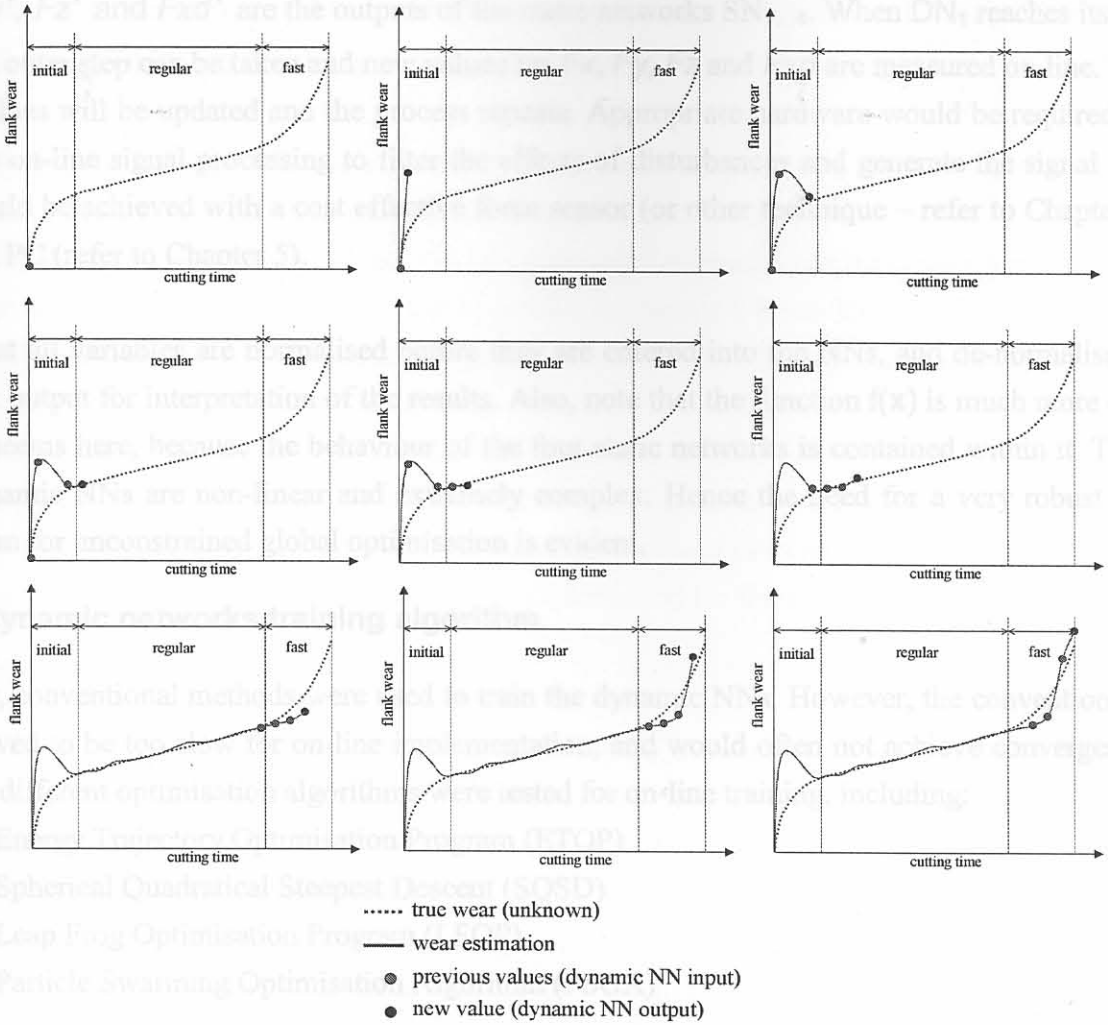

Figure 4.47: Typical behaviour of dynamic NN

Looking at the mathematical formulation, the problem can be described by considering a vector **x** containing the network bias and weight values of DN_1:

$$\mathbf{x} = [x_1\ x_2 \ldots x_n] \tag{4.5}$$

where n is the number of weight and bias values in DN_1. In order to increment an outer step, the following optimisation problem must be solved, which is the training goal of the dynamic NNs:

$$\text{minimise } f(\mathbf{x}) = \sum_{j=1}^{4} e_j \text{ such that } f(\mathbf{x}) \le tol \tag{4.6}$$

with the initialisation space for a new tool starting at:

$$D = \left\{ (x_1 \ldots x_n) \in \Re^n : -1 \le x_i \le 1,\ i = 1..n \right\} \tag{4.7}$$

and *tol* a suitable convergence tolerance on the function value. The design space for a worn tool is taken from the solution of the previous outer step. Initially, all wear values are set to zero. The error functions in Equation 4.6 are defined as:

$$\begin{aligned} e_1 &= \sqrt{(Fx' - Fx)^2} \\ e_2 &= \sqrt{(Fy' - Fy)^2} \\ e_3 &= \sqrt{(Fz' - Fz)^2} \\ e_4 &= \sqrt{(Fxd' - Fxd)^2} \end{aligned} \tag{4.8}$$

Fx', *Fy'*, *Fz'* and *Fxd'* are the outputs of the static networks $SN_{1...4}$. When DN_1 reaches its training goal, an outer step can be taken and new values for *Fx*, *Fy*, *Fz* and *Fxd* are measured on-line. The tool wear values will be updated and the process repeats. Appropriate hardware would be required as well as some on-line signal processing to filter the effects of disturbances and generate the signal features. This could be achieved with a cost effective force sensor (or other technique – refer to Chapters 2 and 5) and a PC (refer to Chapter 5).

Note that all variables are normalised before they are entered into the NNs, and de-normalised at the network output for interpretation of the results. Also, note that the function **f(x)** is much more complex than it seems here, because the behaviour of the four static networks is contained within it. The static and dynamic NNs are non-linear and extremely complex. Hence the need for a very robust and fast algorithm for unconstrained global optimisation is evident.

4.6.4 Dynamic networks training algorithm

Initially, conventional methods were used to train the dynamic NNs. However, the conventional methods proved to be too slow for on-line implementation, and would often not achieve convergence. Numerous different optimisation algorithms were tested for on-line training, including:

- Energy Trajectory Optimisation Program (ETOP)
- Spherical Quadratical Steepest Descent (SQSD)
- Leap Frog Optimisation Program (LFOP)
- Particle Swarming Optimisation Algorithm (PSOA)

A description and a more detailed formulation of the above-mentioned algorithms can be found in Appendix D. The algorithms listed above are all relatively new and unique methods for mathematical optimisation and are especially applicable to engineering-related problems. The formulation of the general mathematical optimisation problem is also documented in Appendix D. After exhaustive investigations, it was found that the Particle Swarming Optimisation Algorithm (PSOA) yielded the best result for training the dynamic NNs. The basic method of particle swarming optimisation was first suggested by Kennedy and Eberhart [224]. Training NNs is in essence an unconstrained global optimisation problem, and recent literature also states that the PSOA outperforms methods like Genetic Algorithms (GAs) in unconstrained global optimisation. The algorithm does not utilise gradient evaluations and its efficient use of random information is advantageous for training NNs. Furthermore the method is easy to implement and computationally efficient. Consider a flock of p particles (or birds). For each particle *i*, Kennedy and Eberhart [224] proposed that the position $\mathbf{x}^i$ be updated as:

$$\mathbf{x}^i_{k+1} = \mathbf{x}^i_k + \mathbf{v}^i_{k+1} \tag{4.9}$$

where **x** represents the position of each bird, **v** the velocity, and *k* a **unit** pseudo-time increment. The velocity $\mathbf{v}^i$ is updated with:

$$\mathbf{v}^i_{k+1} = w\mathbf{v}^i_v + c_1 r_1 \left(\mathbf{p}^i_k - \mathbf{x}^i_k\right) + c_2 r_2 \left(\mathbf{p}^g_k - \mathbf{x}^i_k\right) \tag{4.10}$$

where $\mathbf{p}^i_k$ represents the best ever position of particle *i* at time *k*, and $\mathbf{p}^g_k$ represents the global best position in the swarm at time *k*. The numbers r_1 and r_2 are random uniform numbers between 0 and 1. The

inertia term w is chosen as 1 and then decreased linearly during optimisation. The cognitive and social scaling factors c_1 and c_2 are chosen as $c_1 = c_2 = 2$ in order to allow a mean of unity.

With reference to equation 4.5, the dynamic NN biases and weights were taken as the position vector **x**, and the PSOA solves the optimisation problem described with equation 4.6. In this way, on-line training of the dynamic NN is achieved. On-line training is stopped when f(**x**) reaches the convergence value *tol*. If the convergence criterion is not reached, the vector **x** is randomly re-initialised for a new tool (refer equation 4.7). This is necessary for the case when an old tool is replaced with a new tool, because the swarm moved with the wear of the older tool, and will be too far from the solution to converge within limited steps for a new tool. The algorithm usually achieved convergence within approximately ten inner steps. This is possible in a matter of seconds on a Pentium III processor. If convergence is not achieved within ten steps, the training also terminates and the vector **x** is randomly re-initialised for a new tool. The same procedure is implemented for flank and crater wear.

4.6.5 Results

Results of wear estimations using this technique are shown in Figure 4.48 and Figure 4.49 for experiments 3 and 7, respectively. In each case, the method was tested on previously unseen data. The cutting speeds and feed rates were also included in the static NNs, but were not included in the dynamic NNs. From the results it can be seen that the method estimates the wear values quite accurately, despite the noisy nature of the training and testing data. Hence, the approximate shape and growth of the flank and crater wear can be determined through this method. The effect of a certain quantity of tool wear on the surface and subsurface quality of parts can be obtained from the literature, for example [225]. Thus, a decision can be made whether it would it safe to continue machining or not. In this case, only four estimation results are shown, but the method was successful in estimating the wear of the other experiments (by means of cross-training and cross-validation).

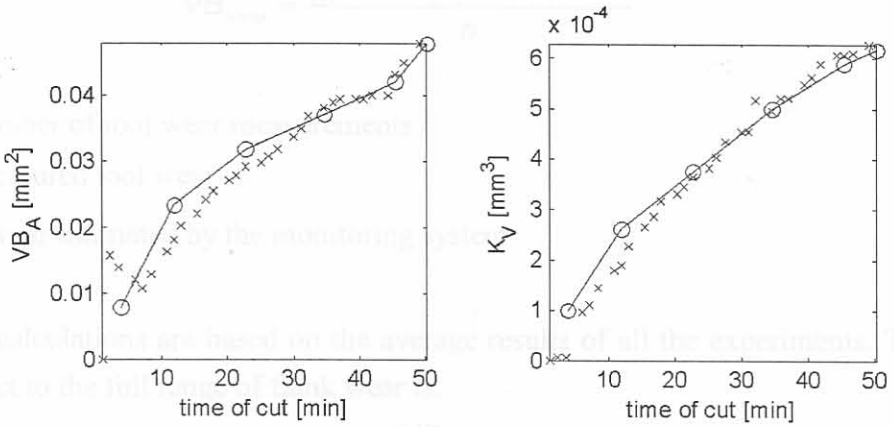

Figure 4.48: Estimation result experiment 3

o = measured values **x** = estimated values

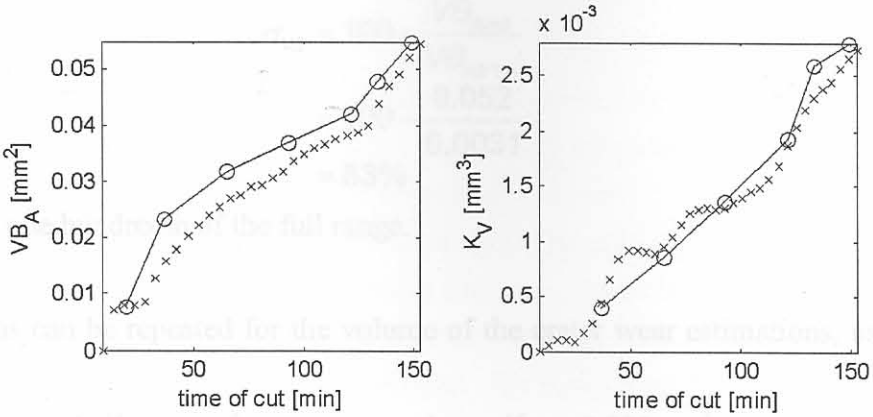

Figure 4.49: Estimation result experiment 7

o = measured values **x** = estimated values

4.6.6 Accuracy

It is essential to evaluate the accuracy of the proposed method if it will be considered for industrial implementation. The following terms and definitions are necessary to evaluate the overall accuracy of the TCMS:

$$\text{Full range of flank wear area } VB_{Afr} = 0.12\text{mm}^2 \tag{4.11}$$

$$\text{Maximum deviation from true wear } VB_{Amd} = 0.01\text{mm}^2 \tag{4.12}$$

$$\text{rms deviation from true wear } VB_{Arms} = 0.0025\text{mm}^2 \tag{4.13}$$

These values were calculated from the results of experiments 1-8.

The rms deviation can be described as:

$$VB_{Arms} = \frac{\sum_{i=1}^{n}\sqrt{(VB_{ATCMS} - VB_{Atrue})_i^2}}{n} \tag{4.14}$$

where:

n = the total number of tool wear measurements

VB_{Atrue} = the measured tool wear

VB_{ATCMS} = the wear estimated by the monitoring system

The following calculations are based on the average results of all the experiments. The average accuracy with respect to the full range of flank wear is:

$$\begin{aligned}\eta_{VB} &= 100 - \frac{VB_{Arms}}{VB_{Afr}} \times 100 \\ &= 100 - \frac{0.0025}{0.12} \times 100 \\ &= 97.9\%\end{aligned} \tag{4.15}$$

The minimum accuracy with respect to the full range of flank wear can be calculated as:

$$\begin{aligned}\sigma_{VB} &= 100 - \frac{VB_{Amd}}{VB_{Afr1\%}} \\ &= 100 - \frac{0.052}{0.0031} \\ &= 83\%\end{aligned} \tag{4.16}$$

where $VB_{Afr1\%}$ is one hundredth of the full range.

These calculations can be repeated for the volume of the crater wear estimations, using the following definitions:

$$\text{Full range of crater wear volume } K_{Vfr} = 0.006\text{mm}^3 \tag{4.17}$$

$$\text{Maximum deviation from true wear } K_{Vmd} = 0.0004\text{mm}^3 \tag{4.18}$$

$$\text{rms deviation from true wear } K_{Vrms} = 0.0001\text{mm}^3 \tag{4.19}$$

The rms deviation can be described as:

$$K_{Vrms} = \frac{\sum_{i=1}^{n} \sqrt{\left(K_{VTCMS} - K_{Vtrue}\right)_i^2}}{n} \tag{4.20}$$

where

n = the total number of tool wear measurements

K_{Vtrue} = the measured tool wear

K_{VTCMS} = the wear estimated by the monitoring system

The following calculations are based on the average results of all the experiments. The average accuracy with respect to the full range of crater wear is:

$$\begin{aligned}\eta_K &= 100 - \frac{K_{Vrms}}{K_{Vfr}} \\ &= 100 - \frac{0.0001}{0.006} \times 100 \\ &= 98.4\%\end{aligned} \tag{4.21}$$

The minimum accuracy with respect to the full range of crater wear can be calculated as:

$$\begin{aligned}\sigma_K &= 100 - \frac{K_{Vmd}}{K_{Vfr}} \times 100 \\ &= 100 - \frac{0.0004}{0.006} \times 100 \\ &= 93.3\%\end{aligned} \tag{4.22}$$

It can thus be stated that the method will estimate the area of flank wear correctly with an average accuracy of 98%, and in extreme cases not less than 83%. For crater wear, the average accuracy is also 98%, and the minimum accuracy is 93%. These calculations are based on all the experiments described in this chapter. It is possible that the accuracy might be lower during industrial implementations of the method, which is described in the next chapter.

4.7 Conclusion

A first important conclusion is that identification and isolation of disturbances on experimental data is essential during hard turning. Furthermore, some parameters influence one another in an unknown and complex manner, and these correlations were identified with a SOM analysis. This assisted in removing the effect of disturbances from the experimental data. The effect of disturbances could be removed from the data with appropriate signal processing methods. Possible features for a wear monitoring method were generated from the force signals after investigating numerous features from force, vibration and AE signals. The best features were selected after examining the effect of machining parameters, machine type and workpiece type on the data.

This chapter also demonstrated how AI could be utilised to effectively monitor crater and flank wear during hard turning. The method is formulated with a combination of static and dynamic NNs, and the training of the dynamic NNs is done with the PSOA. The advantage of this formulation is the fact that the dynamic NNs can follow any progression of wear, and protects the monitoring system against possible disturbances that may cause the system to estimate erroneous values of wear. The behaviour of the dynamic NNs is to follow on its present path, but use information from the force measurements to update its path. Thus, the low signal to noise ratio common to cutting force data has a very small impact on the accuracy of the method.

It was shown that the method is reliable and can be expected to operate with more than 90% accuracy under laboratory conditions. For a shop floor implementation, data from an actual shop floor would be required to verify the accuracy. The method is however applicable to the shop floor due to the low sensitivity towards disturbances. The method was trained for different machining conditions on different machines and it was shown that the method applies to the whole range of experimental conditions. Due to the unique formulation of the proposed AI method, it provides an accurate solution for monitoring crater and flank wear during hard turning. The suggested wear monitoring method is simple and flexible enough for on-line implementation, which will allow more reliable hard turning in industry.